Inorganic Chemistry

Article

pubs.acs.org/IC

Synthesis and Redox Activity of "Clicked" Triazolylbiferrocenyl Polymers, Network Encapsulation of Gold and Silver Nanoparticles and Anion Sensing

Amalia Rapakousiou,[†] Christophe Deraedt,[†] Joseba Irigoyen,[‡] Yanlan Wang,[†] Noël Pinaud,[†] Lionel Salmon,[§] Jaime Ruiz,[†] Sergio Moya,[‡] and Didier Astruc*,[†]

[†]ISM, UMR CNRS No. 5255, Université de Bordeaux, 33405 Talence Cedex, France

[‡]CIC biomaGUNE, Unidad Biosuperficies, Paseo Miramón 182, Edif. "C", 20009 Donostia-San Sebastián, Spain

[§]Laboratoire de Chimie de Coordination UPR CNRS No. 8241, 31077 Toulouse Cedex, France

Supporting Information

ABSTRACT: The design of redox-robust polymers is called for in view of interactions with nanoparticles and surfaces toward applications in nanonetwork design, sensing, and catalysis. Redox-robust triazolylbiferrocenyl (trzBiFc) polymers have been synthesized with the organometallic group in the side chain by ring-opening metathesis polymerization using Grubbs-III catalyst or radical polymerization and with the organometallic group in the main chain by Cu(I) azide alkyne cycloaddition (CuAAC) catalyzed by [Cu(I)(hexabenzyltren)]Br. Oxidation of the trzBiFc polymers with ferricenium hexafluorophosphate yields the stable 35-electron class-II mixed-valent biferrocenium polymer. Oxidation of these polymers with Au^{III} or Ag^{I} gives nanosnake-shaped networks (observed by transmission electron microscopy and atomic force microscopy) of this mixed-valent $Fe^{II}Fe^{III}$ polymer with encapsulated metal nanoparticles (NPs) when the organoiron group is located on the side chain. The factors that are suggested to be synergistically responsible for the NP stabilization and network formation are the polymer bulk, the trz coordination, the nearby cationic charge of trzBiFc, and the inter-BiFc distance. For instance, reduction of such an oxidized trzBiFc-AuNP polymer to the neutral trzBiFc-AuNP polymer with $NaBH_4$ destroys the network, and the product flocculates. The polymers easily provide modified electrodes that sense, via the oxidized $Fe^{II}Fe^{III}$ and $Fe^{III}Fe^{III}$ polymer states, respectively, ATP^{2-} via the outer ferrocenyl units of the polymer and Pd^{II} via the inner Fc units; this recognition works well in dichloromethane, but also to a lesser extent in water with NaCl as the electrolyte.

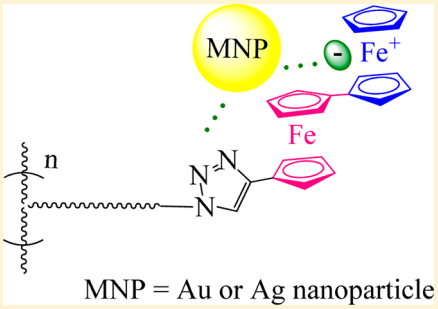

INTRODUCTION

Ferrocene[1] and related iron sandwich complexes[2] have long been shown to possess excellent redox stabilities[3] that have allowed the development of properties and applications in electrochemistry,[4] catalysis,[5] nanomedicine,[6] and sensing.[7] Consequently, metallocene-containing polymers have attracted considerable related attention in materials science.[8] Most of these nanomaterials involve the ferrocene (Fc) prototype; in particular, ring-opening of ferrocenophane monomers directly leads to the synthesis of Fc polymers and herewith to the controlled design of mono- and bidimentional nanomaterials.[9] Despite the well-known stability of the d^5 17-electron ferricenium cation,[1] many ferricenium compounds are fragile and air-sensitive in organic solutions.[10] Therefore, we have investigated the synthesis of metallopolymers based on the biferrocene (BiFc) unit[11] because the stereoelectronic stabilization of the mixed valency in cationic biferrocenium derivatives leads to much more robust nanomaterials than with single ferricenium groups. BiFc redox chemistry includes three easily accessible oxidation states, and the biferrocenium cation belongs to class II of the Robin and Day classification with valence localization at the infrared time scale.[12] BiFc has been incorporated into nanosystems such as gold nanoparticles (AuNPs) for electrodeposition[13] and dendrimers for "molecular printboards,"[14] fabrication of molecular junctions[15] and further studies of their redox properties.[16] However, the multielectron properties of BiFc polymers[17] have not yet been much studied, and the remarkable availability and stability of biferrocenium polymers allow the design of useful redox reactions starting from BiFc polymers and leading to original nanomaterials and their networks.

A breakthrough in the monofunctionalization of BiFc was the synthesis of ethynylbiferrocene allowing the easy incorporation of BiFc moieties into dendrimers and gold nanoparticles by Sonogashira, homocoupling or "click" reactions.[18] The latter reaction introduces the 1,2,3-triazolyl (trz) group that is very useful for various applications including redox recognition, coordination to transition-metal cations, and stabilization of AuNPs and PdNPs for catalysis,[19] is biocompatible.[20] Indeed, triazolylbiferrocenyl (trzBiFc) dendrimers proved to be excellent selective exoreceptors in the homogeneous phase, as

Received: December 5, 2014
Published: February 13, 2015

DOI: 10.1021/ic5028916
Inorg. Chem. 2015, 54, 2284−2299

Scheme 1. Synthesis of Ethynylbiferrocene 3

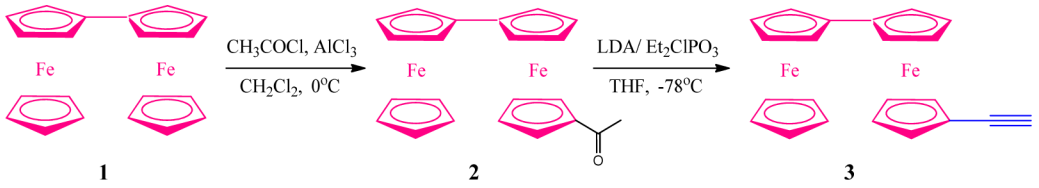

Scheme 2. Synthesis of the trz-BiFc-Functionalized Norbornene Monomer 7

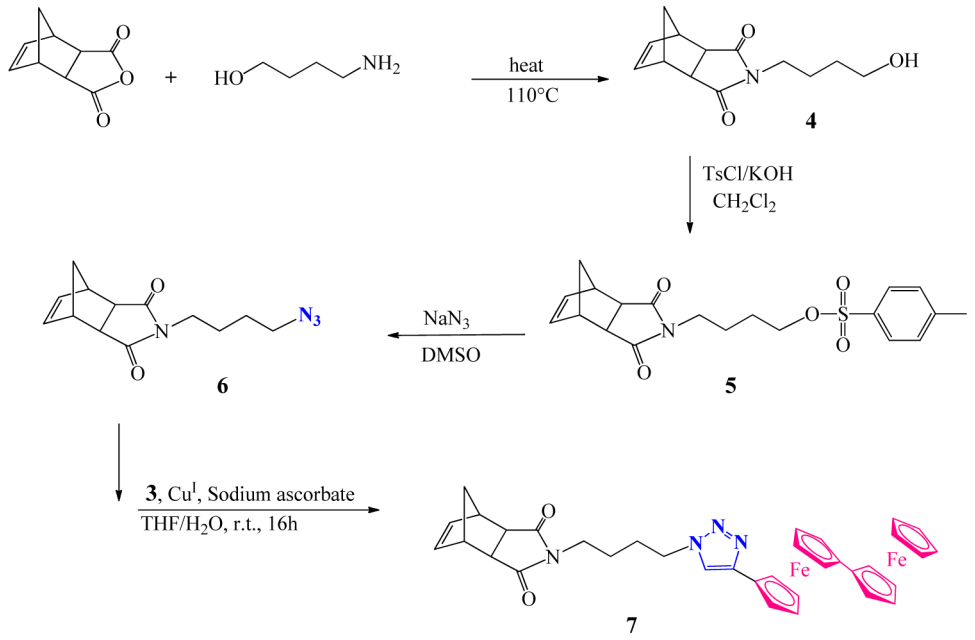

the outer Fc moiety could recognize oxo-anions, whereas the inner Fc recognized transition-metal cations.[18b,c] However, these molecular tools should be immobilized onto solid surfaces in order to be incorporated in electrochemical sensing devices. Following this strategy we envisaged extending the "click" BiFc functionalization to polymers by preparing easily accessible trzBiFc polymers and copolymers with polyethylene glycol chains as co-units using ring-opening metathesis polymerization (ROMP), copper-catalyzed azide alkyne cycloaddition (CuAAC, "click") polycondensation and free-radical polymerization.[21] The full characterization of these metallopolymers by ^{1}H, ^{13}C, HSQC, HMBC, COSY and NOESY, DOSY NMR spectroscopy is shown here including infrared, UV−vis, dynamic light scattering (DLS), size exclusion chromatography (SEC), matrix assisted laser desorption ionization time-of-flight (MALDI-TOF) mass spectrometry, and cyclic voltammetry (CV). Oxidation of the metallopolymers using $HAuCl_4$ leads to mixed-valent trz-biferrocenium polymers that encapsulate AuNPs and AgNPs in snake-shaped networks, as shown by transmission electron microscopy (TEM), atomic force microscopy (AFM), UV−vis, DLS, IR, near-IR and CV. The new trzBiFc-terminated metallopolymers were used to derivatize Pt electrodes for redox recognition of ATP^{2-} and Pd^{2+} in organic and aqueous media.

RESULTS AND DISCUSSION

Synthesis and Characterization of triazolylBiFc Polymers 9, 10, 14, 18, and 19. *Synthesis of Ethynylbiferrocene 3.* Ethynylbiferrocene **3** was synthesized in two steps from BiFc,[22] **1**. (Scheme 1). The first step is the synthesis of acetylbiferrocene **2** that consists of a Friedel−Crafts acetylation of BiFc and is based on the work by Doisneau et al. that was reported in 1992.[23] Ethynylbiferrocene[18e] **3** was subsequently prepared in a reaction similar to that used for the synthesis of ethynylferrocene[24] between acetylbiferrocene and lithiumdiisopropylamide (LDA)/diethylchlorophosphate followed by column chromatography with pentane as eluent. This provided **3** as an orange crystalline powder in a 50% overall yield from BiFc.

Synthesis of the trzBiFc-Functionalized Norbornene Monomer 7. Commercial *cis*-5-norbornene-*exo*-2,3-dicarboxylic anhydride reacts at 110 °C with 4-aminobutanol to give the 4-hydroxylbutyl-*cis*-5-norbornene-exo-2,3-dicarboximide in quantitative yield.[25] Then under basic conditions the nucleophilic substitution of **4** by TsCl (Ts = tosyl) gives **5**, and nucleophilic substitution of tosyl by azide yields the azidonorbornene monomer **6**. Then CuAAC reaction between ethynylbiferrocene and monomer **6** catalyzed by Cu(I) leads to the trz-BiFc-functionalized norbornene monomer **7** in 97% yield (Scheme 2). After purification, compounds **5**, **6**, and **7** are identified and characterized by ^{1}H and ^{13}C NMR and IR spectroscopy, electrospray ionization mass spectrometry (ESI MS), UV−vis, elemental analysis, and CV. The ^{1}H NMR spectrum of **5** shows the appearance of the four tosylate protons at 7.74 and 7.31 ppm and the $-CH_2OTs$ protons at 3.97 ppm, whereas in compound **6** the four protons of the tosylate groups are no longer observed, and the new $-CH_2N_3$ peak appears at 3.47 ppm. The appearance of a strong absorption band at 2097 cm^{-1} is observed in the IR spectrum corresponding to the $-N_3$ group. After the "click" reaction, the triazolyl proton appears at

DOI: 10.1021/ic5028916
Inorg. Chem. 2015, 54, 2284−2299

Scheme 3. ROMP Reaction of the trzBiFc Norbornene Monomer 7

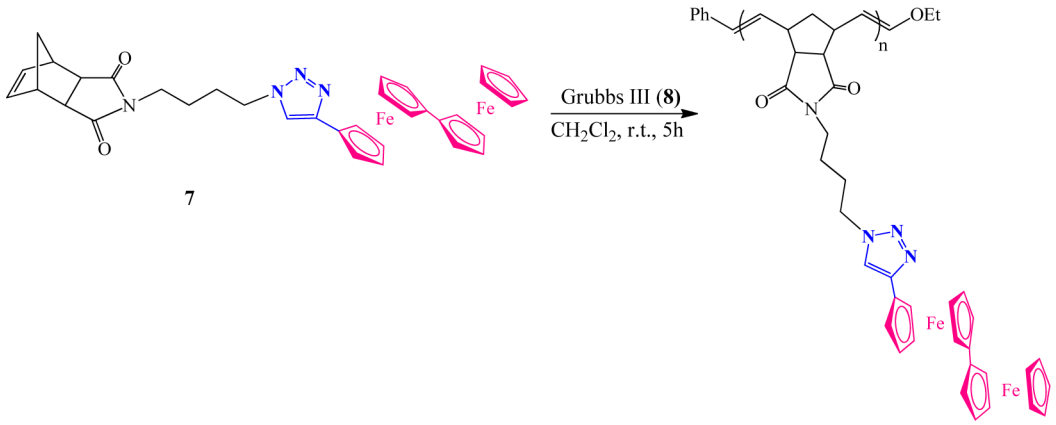

7.03 ppm, and the $-CH_2$trz peak is deshielded at 4.50 ppm because of the electron-withdrawing property of the trz group. The $-N_3$ absorption band in the IR is no longer observed, indicating the disappearance of the starting material **6**. The UV−vis spectrum recorded in dichloromethane (DCM) shows a strong absorption at λ_{max} = 450 nm (Supporting Information, S20) due to the d−d* transitions of BiFc. Finally, ESI MS and elemental analysis confirm the molecular structure of **7**.

Ring-Opening-Metathesis Polymerization of the Norbornene Functionalized with a trzBiFc Group. The polymerization of the trzBiFc-substituted norbornene monomer **7** (Scheme 3) proceeds in distilled DCM in the presence of the third-generation of Grubbs' Ru metathesis catalyst (called Grubbs III, **8**,[26] Figure 1) at r.t. in 5 h.

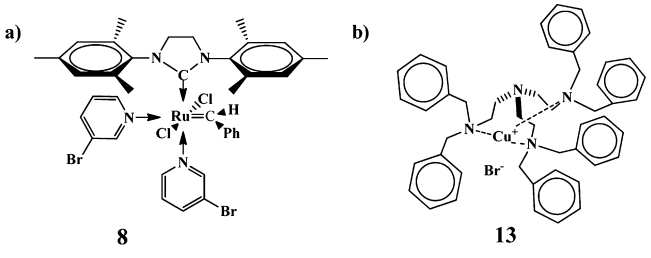

Figure 1. (a) Third generation Ru metathesis catalyst, Grubbs III (**8**) (b) CuACC catalyst copper [Cu^{I}tren$(CH_2Ph)_6$][Br] (**13**).

Then excess ethyl vinyl ether is added to quench the reaction. The use of monomer/catalyst ratios of 30 and 60 respectively gives polymers **9** and **10** in 98% and 99% yield, as bright orange crystalline solids (Scheme 3). Various concentrations of the monomer are examined for the ROMP polymerization of monomer **7**, and the optimal conditions (highest conversion in a shorter time) are achieved when the concentration of monomer **7** is ≥0.25 M.

^{1}H NMR is a key tool to check whether the polymerization is finished. Indeed the olefinic protons that are found at 6.3 ppm in monomer **7** are now displaced to the region of 5.5−5.8 ppm after polymerization. The bulky nature of the trzBiFc group is also shown by ^{1}H NMR for polymers **9** and **10**. The trz proton that is represented by a single peak in monomer **7** is split into a doublet due to two distinct sterically hindered conformations of the BiFc units composing polymers **9** and **10**. For instance, in HSQC 2D NMR for polymer **9** both trz proton peaks correspond to the single −CH carbon peak of trz at 119.85 ppm, and in HMBC 2D NMR they both correspond to the $-Cq$ of trz at 145.31 ppm. Interestingly, NOESY 2D NMR shows that only one of the two peaks representing the trz proton is correlated to the substituted protons of the BiFc group. The protons of the alkyl chain and the $-CH_2$CH of the NBR part indicate that some trz units are spatially close to the polymeric chain, whereas others are not spatially constrained. Last, the phenyl group of the catalyst is located at the end of the polymer chain after polymerization. This phenyl group is found in the area of 7.20−7.40 ppm that is merged with that of the trz proton. However, extracting the assignment of this area (7.1−7.4 ppm) allows the rough estimation of the number of units of polymers **9** and **10** by end-group analysis that is in accordance with the theoretical values (30 and 60 units respectively) (Supporting Information, S22 and S35). The IR spectrum shows the characteristic band of the C═O stretching that is found at 1698 cm^{-1}. Additionally, a strong absorption band is found at 816 cm^{-1} that is a characteristic frequency of the C−H out-of-plane bending vibration of ferrocene. Finally, the absorption due to the ═C−H stretching of the trz and the Cp groups of the trzBiFc units is found at around 3090 cm^{-1}.

Synthesis of the trzBiFc Polystyrene ***14***. Poly(biferrocenylmethylstyrene) **14** is synthesized in an easy three-step reaction (Scheme 4). First, poly(chloromethylstyrene) polymer **11** is prepared by free-radical polymerization of commercial chloromethylstyrene using 0.5% of AIBN as the initiator (Scheme 4), a reaction that takes place in toluene at 80 °C. Nucleophilic substitution of the chloro groups using sodium azide yields 85% of the azido-polymer **12**.[27]

The two polymer precursors **11** and **12** are analyzed by SEC which shows the molecular weight distribution curve of **11** with a polydispersity index (PDI) = 1.40 and **12** with PDI = 1.25. The polydispersity is easily improved from **11** to **12** after the azidation reaction by precipitation of **12** in MeOH twice. Molecular weight data using polystyrene as the standard reference show that polymer **12** consists of 31 units. The IR spectrum (KBr) shows a strong band at 2097 cm^{-1} attributed to the $-N_3$ absorption of **12**.

The third step of the synthesis of polymer **14** is the CuAAC functionalization of the poly(azidomethylstyrene) polymer with multiple trzBiFc units. The most common Cu^{I} catalyst used for this reaction is copper sulfate that is reduced in situ by sodium

DOI: 10.1021/ic5028916
Inorg. Chem. 2015, 54, 2284−2299

Scheme 4. Synthesis of the Poly(trz-BiFc-methylstyrene) 14

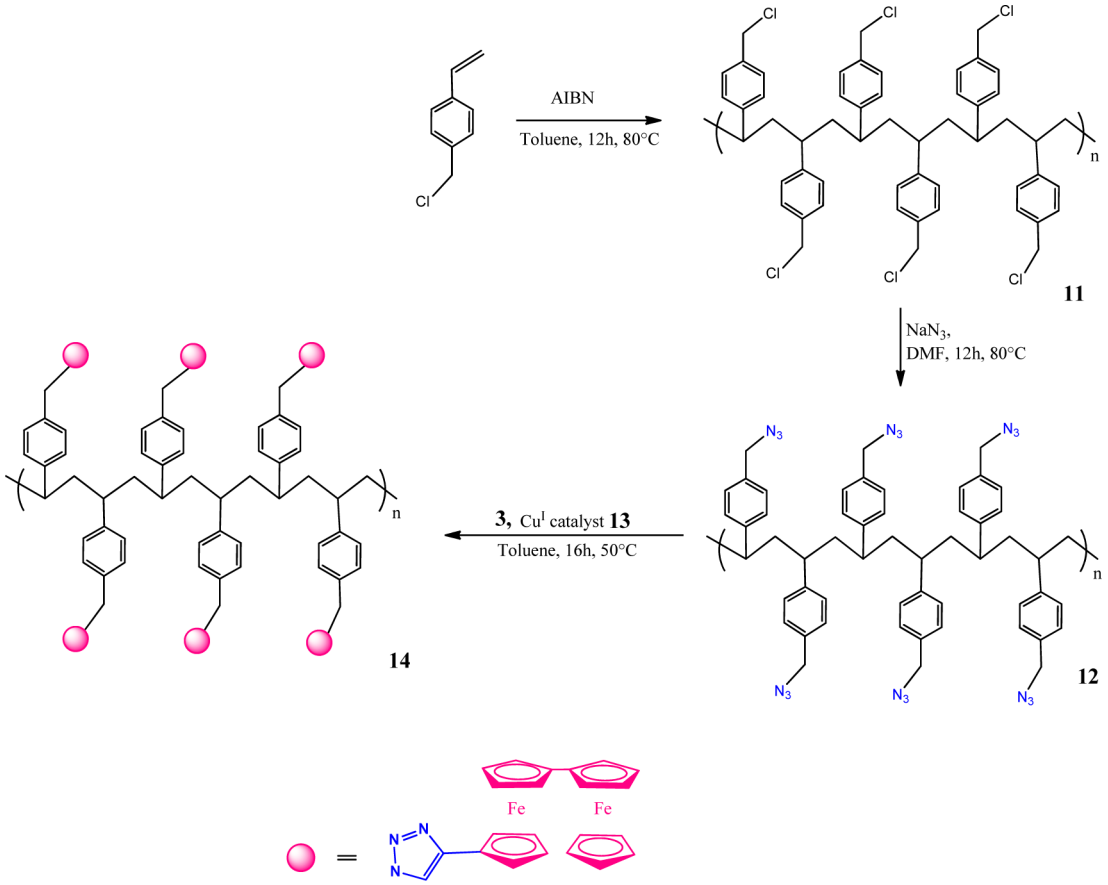

Scheme 5. Synthesis of the Poly-trzBiFc-PEG Polymers 18 and 19

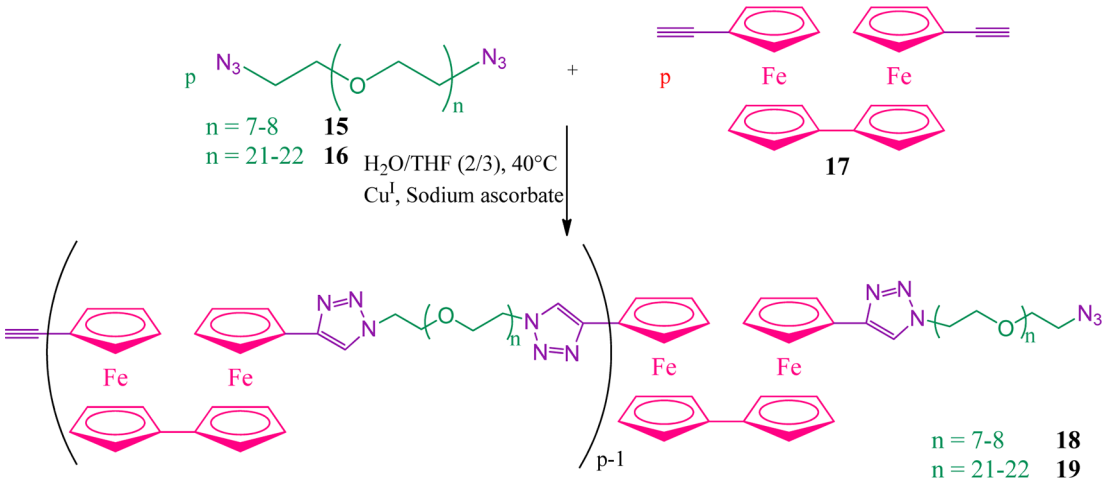

ascorbate from Cu^{II} to Cu^{I}.[28] However, it is unsuitable for macromolecules with multiple azide groups such as dendrimers, polymers, or nanoparticles, leading to lower reaction rates and lower yields, and other catalysts are envisaged.[29] Additionally stoichiometric amounts of the "catalyst" $CuSO_4{\cdot}5H_2O$ are required, with difficulties for the separation of the remaining catalyst that remains trapped inside the macromolecule at the multiple trz units.[30] Recently the CuAAC catalyst [Cu(I)-(hexabenzyl)tren]Br **13** (Figure 1b) was reported with excellent efficiency, including for synthesis of dendrimers[31] and gold nanoparticles.[32]

Consequently, polymer **14** is successfully synthesized by CuAAC reaction between ethynylbiferrocene **3** and the azido polymer **12** using 15% of catalyst **13**. The reaction occurs at 60 °C under nitrogen in toluene in which the precursors **3** and **12** as well as the catalyst **13** are very soluble. After 16 h, the polymer **14** is formed in 97% yield as an orange precipitate allowing its easy separation from the catalyst **13** that remains in toluene solution. The IR characteristic absorption of the azido groups in the region of 2094 cm^{-1} of poly-azido precursor **12** disappears completely at the end of the reaction, confirming that all the azido groups are replaced by trz groups. NMR

DOI: 10.1021/ic5028916
Inorg. Chem. 2015, 54, 2284−2299

spectroscopy confirms the structure of the poly-trzBiFc polymer **14**. Specifically, the formation of the trz unit is shown in the ^{1}H NMR spectrum by the appearance of the proton peaks at 7.68 ppm corresponding to the proton of the trz unit. The CH_2-N_3 protons for precursor **12** at 4.25 ppm are replaced by the CH_2-trz at 5.41 ppm. The other characteristic peaks of the polymer **14** are also observed, and the correct ratio between polymer/BiFc protons finally confirms the structure of compound **14**. Last, ^{13}C NMR shows the characteristic peaks of *Cq*, CH of trz, and CH_2-trz of the polymer **14**.

*Synthesis of Triazolyl-biferrocenyl-PEG Copolymers **18** and **19**.*[17c] The copolymers containing both biferrocene and PEG units are synthesized by "click" CuAAC polycondensation reactions (Scheme 5).

The CuAAC reactions take place between the bis-azido-PEG derivatives **15** and **16** that contain 7−8 and 21−22 ethylene glycol units respectively and bis-ethynyl-BiFc[33] in a mixture of THF/H_2O, at 40 °C for 2 days. The use of the Sharpless-Fokin catalyst $CuSO_4{\cdot}5H_2O$ + Na ascorbate leads to the polymers **18** and **19** in 78% and 58% yield, respectively. Both polymers were purified by precipitation in diethyl ether twice. The introduction of several PEG units in polymeric materials is of interest for biocompatibility, water-solubility, and enhanced permeation and retention (EPR).[34] Polymer **18** containing PEG units of molecular weight 400 Da presents solubility properties that are similar to those of the homopolymers **9**, **10**, and **14**, whereas polymer **19** containing PEG units of molecular weight 1000 is also soluble in very polar solvents including water. The ^{1}H NMR and ^{13}C NMR spectra confirm the structures of the copolymers **18** and **19**, whereas IR spectroscopy indicates the absence of trace of azide or alkyne groups, suggesting that these polymers consist of several units without the possibility to observe the end groups.

The HSQC, HMBC, and COSY NMR spectra helped to make the correct assignments of proton and carbon signals for all the series of trzBiFc polymers **9**, **10**, **14**, **18**, and **19**. The objective of DOSY NMR is double: measure the hydrodynamic diameter of the polymers in solution and obtain a DOSY spectrum that reflects the purity of the polymers. The DOSY NMR spectra of the polymers **9**, **10**, **14**, **18**, and **19** are obtained as well as their diffusion coefficient (Supporting Information). The higher the molecular weight of the polymer, the smaller the diffusion coefficient and the larger the hydrodynamic diameter; the latter is calculated using the Stokes−Einstein equation $D = K_BT/6\pi\eta r_H$. The largest r_H value, 13.1 ± 1.0 nm, is calculated for the copolymer **19**, whereas the smallest r_H value, 1.5 ± 0.5 nm, is calculated for the polymer **9**. Finally, DLS also gives access to the hydrodynamic diameter of the polymers **9**, **10**, and **14** that are d_1 = 14.3 ± 3 nm, d_2 = 36.9 ± 7 nm, and d_3 = 11.9 ± 2 nm, respectively.

The MALDI-TOF mass spectra of the polymers **9** and **14** show well-defined individual peaks for polymers fragments that are separated by 654 ± 1 Da (polymer **9**) and 553 ± 2 Da (polymer **14**) corresponding to the mass of a single unit of the corresponding polymers. The the most intense molecular peak, 13990.1 Da, obtained for polymer **14**, corresponds to a polymer fraction of 25 trzBiFc units. The intensities of the peaks, separated by 654 ± 1 Da (polymer **9**) or 553 ± 2 Da (polymer **14**), progressively decrease and vanish toward higher molecular masses. The same phenomenon is observed for the copolymer **18**, where the repetition of peaks for polymer fragments are separated by approximately 800 ± 50 Da, as it is known that PEG400 (part of precursor **15**) is an average number of several lengths of PEG fragments. These MALDI-TOF mass spectra clearly show the structure and motifs of polymers **9**, **14**, and **18**.

All the polymers were also characterized by UV−vis. spectra in which a strong absorption band is observed in the visible region peaking at 450−451 nm due to the d−d* transitions of BiFc and is typical of BiFc compounds.[35] The molar extinction coefficients ε of all polymers are calculated from Lambert's-Beer law $A = \varepsilon bc$ (Table 2).

SEC of the trzBiFc polymers **9**, **10**, **14**, **18**, and **19** provides PDI = 1.21−1.27, the smallest PDI value being observed for the ROMP polymers **9** and **10** as expected. The M_w values that are obtained from SEC in all cases indicate polymers that are not in accord with the expected molecular weights, having fewer trzBiFc units. It is possible that these polymers interact with the column phase inducing a longer retention time and a smaller molecular weight. The calculated molecular weights are discussed below and gathered in Table 2.

CV usually provides information on the ligand electronic effect;[36] here it is used for polymers **9**, **10**, **14**, **18**, and **19** with decamethylferrocene, $FeCp^*_2$ ($Cp^* = \eta^5$-C_5Me_5), as the internal reference[37] in order to examine the thermodynamics and kinetics of the heterogeneous electron-transfer processes, the stability of the oxidized states and finally estimate the number of monomer units in the polymers. The CVs are recorded in CH_2Cl_2, a good solubility being accessible with this solvent for all polymers, on a Pt electrode, using 0.1 M $[n\mathrm{Bu_4N}][PF_6]$ as the supporting electrolyte. All polymers show two reversible waves vs $FeCp^*_2$. The first oxidation wave of polymers **9**, **10**, **14**, **18**, and **19** corresponds to the oxidation of the first Fc center to the mixed-valent 35-electron complex $Fe^{II}Fe^{III}$ biferrocenium, and the second wave corresponds to the oxidation of the second Fc center to the 34-electron $Fe^{III}Fe^{III}$ biferricenium species.

The BiFc groups of the trz-BiFc polymers give two single waves, which indicates that there is no interaction between different BiFc units; this is explained by the weakness of the electrostatic factor between the redox sites of the trzBiFc polymers because these redox centers are far from one another, being separated by many bonds.[38]

The electrochemical reversibility of the CV waves of all the redox groups signifying fast electron transfer between these redox groups and the electrode is due to very fast access of these groups to the electrode within the electrochemical time scale, all the redox groups coming in turn close to the electrode,[39] and/or the electron-hopping mechanism.[40]

For polymers **9**, **10**, and **14** containing side BiFc chains the first oxidation wave is assigned to the outer Fc groups that are easier to oxidize than the inner ones, as they bear only the electron-releasing inner Fc groups, whereas the second oxidation wave is assigned to the inner Fc groups that bear the electron-withdrawing trz substituents (Table 1).

Adsorption during CV that is common for redox-active macromolecules[41] is observed for all polymers studied here. The $\Delta(E_{pc} - E_{pa})$ value is <59 mV, signifying partial adsorption on the electrode surface. In Figure 2a,b the CVs of monomer **7** and polymer **9** are shown where the adsorption is clear in polymer **9** even from the first scan, whereas as expected it is not observed for monomer **7**. This facile adsorption favors the easy fabrication of metallopolymer-modified electrodes. In Figure 2c, progressive adsorption on the Pt-electrode of polymer **9** is demonstrated after approximately 20 scans around the potential region of the BiFc CV waves. The same phenomenon is observed for all polymers, except for polymer **19** probably due

DOI: 10.1021/ic5028916
Inorg. Chem. 2015, 54, 2284−2299

Table 1. Redox Potentials and Chemical (i_c/i_a) and Electrochemical ($E_{pa} - E_{pc} = \Delta E$) Reversibility Data for Monomers 3, 7, and 17 and for Polymers 9, 10, 14, 18, and 19[a]

compound	$E_{1/2}$ (V)[b]	ΔE (mV)[b]	i_c/i_a[b]	$E_{1/2}$ (V)[c]	ΔE (mV)[c]	i_c/i_a[c]
3	0.48	59	1.0	0.93	56	1
7	0.43	50	1.1	0.79	40	0.8
9	0.42	15	1.1	0.76	20	1.4
10	0.42	30	1.8	0.74	20	1.3
14	0.41	10	1.7	0.72	15	1.5
17	0.58	60	1.1	0.93	55	1.0
18	0.44	55	1.4	0.79	40	1.5
19	0.42	35	1.3	0.80	45	1.0

[a]Supporting electrolyte: [*n*-Bu_4N][PF_6] 0.1 M; solvent: dry CH_2Cl_2; working and counter electrodes: Pt; reference electrode: Ag; internal reference: $FeCp^*_2$; scan rate: 0.200 $V.s^{-1}$. [b]Data obtained for the first wave ($Fe^{II/III}$). [c]Data obtained for the second wave ($Fe^{II/III}$).

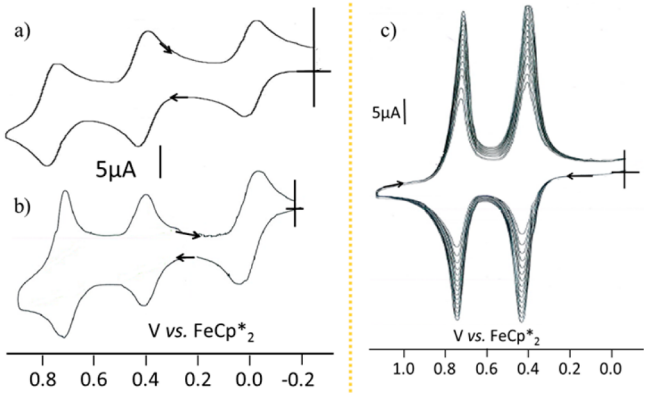

Figure 2. CVs of (a) monomer **7**, (b) polymer **9**, and (c) progressive adsorption of polymer **9** onto a Pt electrode upon 20 scans around the BiFc potentials. Solvent: DCM; reference electrode: Ag; working and counter electrodes: Pt; scan rate: 0.2 V/s; supporting electrolyte: 0.1 M [*n*-Bu_4N][PF_6]. The wave at 0.0 V belongs to the internal reference $FeCp^*_2$.

to the long PEG units that increase the solubility. This adsorption phenomenon for polymers **9**, **10**, and **18** progresses until 27 ± 4 scans, and then a decay of the CV waves progressively takes place presumably due to a structural rearrangement of the polymers on the electrode surface. Surprisingly this is not the case for polymer **14** where the adsorption phenomenon continues until at least 60 scans without any structural rearrangement on the surface of the electrode, which makes polymer **14** an ideal candidate for the fabrication of modified electrodes.

Molecular Weights of Polymers 9, 10, 14, 18, and 19. Different techniques are used for the calculation of the molecular weights of the trzBiFc polymers. For the polymers **9** and **10** that are synthesized by ROMP the end-group (^{1}H NMR) analysis allows the approximate determination of the number of units in these polymers and consequently their molecular weight (Table 2). For polymer **9** the molecular weight determined by this method is M_n = 22 000 g/mol, whereas for the larger polymer **10** the calculated molecular weight is M_n = 36000 g/mol. For both polymers the calculated molecular weights are close to the theoretical ones determined by the monomer/catalyst molar ratio. SEC analysis (vs. polystyrene reference) of the precursor polystyrene polymer **12** is a more viable method to determine the total number of

Table 2. Sizes of the Polymers 9, 10, 14, 18, 19 (Number of Molecular Units) Obtained from End-Group Analysis, CV Analyses and UV-vis Spectroscopy

compound	conversion (%)	n_t[a]/n_p[c]	n_e[d]	n_m[f]
Mono **7**		1		
Poly **9**	98	30/33 ± 4	32 ± 3	33 ± 4
Poly **10**	99	60/55 ± 7	66 ± 6	53 ± 7
Poly **14**	97	31[b]/–	36 ± 4	29 ± 3
Poly **18**	78		151 ± 23[e]	*g*
Poly **19**	58		62 ± 12[e]	*g*

[a]Theoretical number of branches corresponding to [M]/[C] molar ratio. [b]Obtained from the SEC analysis of the organic precursor **12** (using polystyrene as standard). [c]Values obtained by ^{1}H NMR end-group analysis in CD_2Cl_2, at 25 °C. [d]Number of electrons obtained by CV from eq 2. [e]Molecular weight of polymers **18** and **19** were calculated by eq 1 upon using the diffusion coefficients obtained from DOSY NMR analysis. [f]Number of metallocene units obtained by UV–vis. spectroscopy using equation: $n_m = \varepsilon/\varepsilon_o$. [g]The equation $n_m = \varepsilon/\varepsilon_o$ is not adequate for polymers **18** and **19** because of the existence of the PEG units.

units, giving a molecular weight of 4938 g/mol corresponding to 31 units. As the CuAAC reaction of precursor **12** with compound **3** is complete (no $-N_3$ absorption in the IR after the reaction) and the PDIs of **12** and **14** are the same, the number of trzBiFc units in this case remains the same as the number of azido groups in polymer **12**.

CV also is a valuable tool for the estimation of the number of units in the trzBFc polymers **9**, **10**, **14**, **18**, and **19**. The total number of electrons transferred in the oxidation wave for the polymer (n_e) can be estimated from the limiting currents and approximate relative values of the diffusion coefficients of the monomer (D_m) and the polymer (D_p):

$$D_p/D_m = (M_m/M_p)^{0.55} \quad (1)$$

Since the oxidation of each redox moiety is a one-electron reaction ($Fe^{II} \rightarrow Fe^{III}$), the value of n_e can be estimated by employing Bard's equation previously derived for conventional polarography:[41,42]

$$n_e = (i_{dp}/C_p)/(i_{dm}/C_m)(M_p/M_m)^{0.275} \text{ (ref 42)} \quad (2)$$

Consequently comparison with the internal reference $FeCp^*_2$ provides a good estimation of the number of electrons n_p involved in the $Fe^{II/III}$ redox process as a function of the monomer and polymer intensities (i), concentrations (c), and molecular weights (M). Measurement of the respective intensities for the reference $FeCp^*_2$ and the first anodic wave (see Supporting Information for the CVs with $FeCp^*_2$ as the reference) led to the data of n_e for the polymers **9**, **10**, **14**, **18**, and **19.** The n_e values of polymers **9**, **10**, and **14** are slightly superior to the theoretical number of polymeric units, probably due to their slight adsorption on the Pt electrode starting even from the first scan around the BiFc potentials. For copolymers **18** and **19**, the molecular weight was calculated only by this electrochemical method by both eqs 1 and 2 by using the diffusion coefficients of the monometallic reference $FeCp^*_2$ and polymers **18** and **19**.

UV–vis spectroscopy was used to confirm the number of units in the polymers in all cases. The Lambert–Beer law $A = \varepsilon bc$ was used to determine the actual total number of metallocene (BiFc) groups in polymers **9**, **10**, and **14**. The UV–vis spectra of the polymers present an absorption band at

DOI: 10.1021/ic5028916
Inorg. Chem. 2015, 54, 2284–2299

Scheme 6. Synthesis of Gold Vermicular AuNSs from Polymers 9, 10, and 14[a]

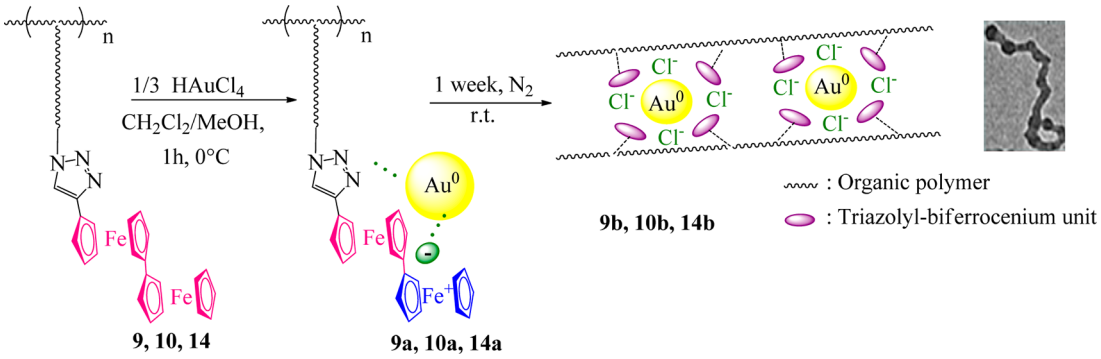

[a]Photograph: isolated vermicular from the TEM analysis of **AuNSs-14b**.

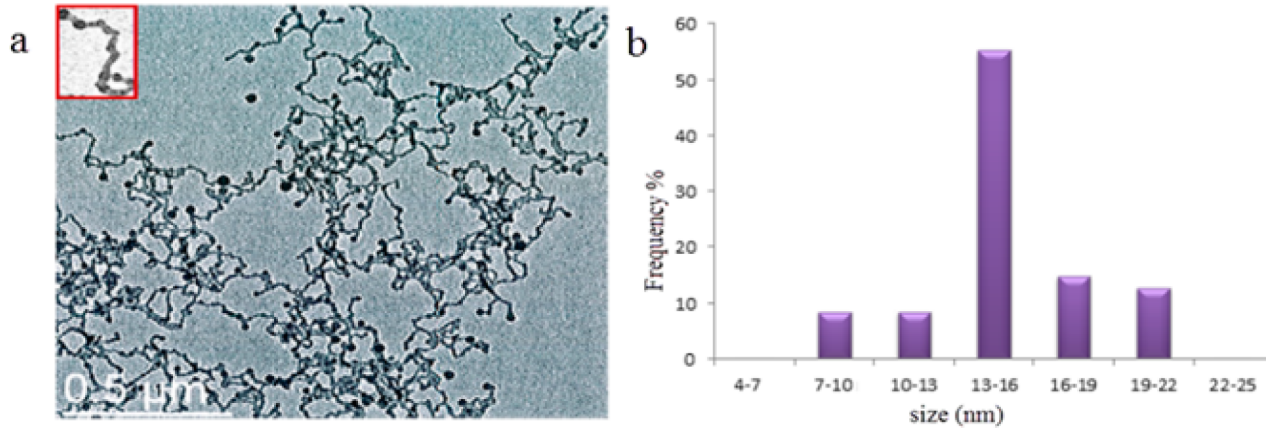

Figure 3. (a) TEM analysis of mixed-valent biferrocenium polymer-stabilized **AuNSs-14b** at 0.5 μm; (b) size distribution of the AuNPs.

450 nm due to the d−d* transitions of BiFc. The number of BiFc termini in each polymer is estimated by comparing the molar extinction coefficient (ε) of the polymers with that of the corresponding monomer (ε_0).[43] The mono-trzBiFc monomer **7** was used for this comparison. The number of metallocenes found in each polymer (**9**, **10**, **14**) confirms the molecular weights calculated with the other methods.

Reaction of Polymers with Au^{III}: Formation of Mixed-Valent Polymers and Stabilization of Encapsulated Gold Nanoparticles by Snake-Shaped Nanonetworks. The BiFc polymers are stoichiometrically oxidized by 1 equiv of ferricenium tetrafluoroborate *per* BiFc unit to robust cationic mixed-valent biferrocenium[43] polymers **18a** and **19a** that are characterized by UV−vis, FT-IR, near-IR, and Mössbauer spectroscopy. The IR spectra of **18a** and **19a** show both ν_{Fc} and ν_{Fc}^{+} at 818 and 833 cm^{-1} indicating that the mixed-valent polymers **18a** and **19a** are localized on the time scale of the molecular vibrations. These two mixed-valent polymers present a band in the near-IR region (at λ_{max} = 1954 and λ_{max} = 1921 nm) indicating that they belong to class II of mixed-valent compounds in the Robin-Day's classification. Mössbauer spectroscopy finally confirms that these two polyelectrolytes **18a** and **19a** are localized class-II mixed-valent complexes.[17c]

The reducing power of the BiFc polymers and the stability of cationic biferrocenium polymers **9**, **10**, and **14** are attractive in view of Au^{III} reduction to Au^0 nanoparticles (AuNPs)[45] that are stabilized in the biferrocenium polymer frameworks.[21,44] Consequently, $HAuCl_4$ is chosen as the oxidant of the outer Fc groups of the trz-BiFc polymers, the reaction being described by eq 3 with the successful stabilization of AuNPs:

$$3Fe^{II}Fe^{II} + H^{+}Au^{III}Cl_4^{-} \rightarrow 3[Fe^{II}Fe^{III}]^{+}Cl^{-}, Au^0, H^{+}Cl^{-} \quad (3)$$

The reactions proceed in a DCM/methanol medium (Scheme 6). The polymer reductant is added dropwise into the $HAuCl_4$ methanol solution, and the color immediately turns from orange-yellow to green suggesting the formation of the mixed-valent polymers **9a**, **10a**, **14a**. The factors that provide AuNP stabilization are mild ligands (trz) at the AuNP surface, electrostatic (chloride counteranions and biferrocenium cations), and steric (bulky biferrocenium units and the polymer frameworks). Surprisingly, a one-week incubation time of the AuNPs stabilized by the mixed-valent biferrocenium polymers progressively leads to the formation of polymer vermicular that encapsulate AuNPs in **9b**, **10b**, and **14b** (Scheme 6).

These peculiar AuNP-encapsulating vermicular networks are clearly seen by TEM analysis (Figure 3, polymer **14**). The average diameter of these **AuNSs-14b** is d = 14.5 ± 1.5 nm, and the calculated distribution of the sizes is shown in Figure 3c. The inter-nanoparticle distance stabilized in the several vermiculars is r = 13.5 ± 1.5 nm (for statistical distribution see Supporting Information). In the red caption of Figure 3a (zoom), an isolated polymer vermicular (AuNS) is shown (length: 269 ± 10 nm; thickness: 8.5 ± 2 nm containing 14 AuNPs). UV−vis spectroscopy characterizes the AuNPs with the classic plasmon band absorption at 531 nm.

DOI: 10.1021/ic5028916
Inorg. Chem. 2015, 54, 2284−2299

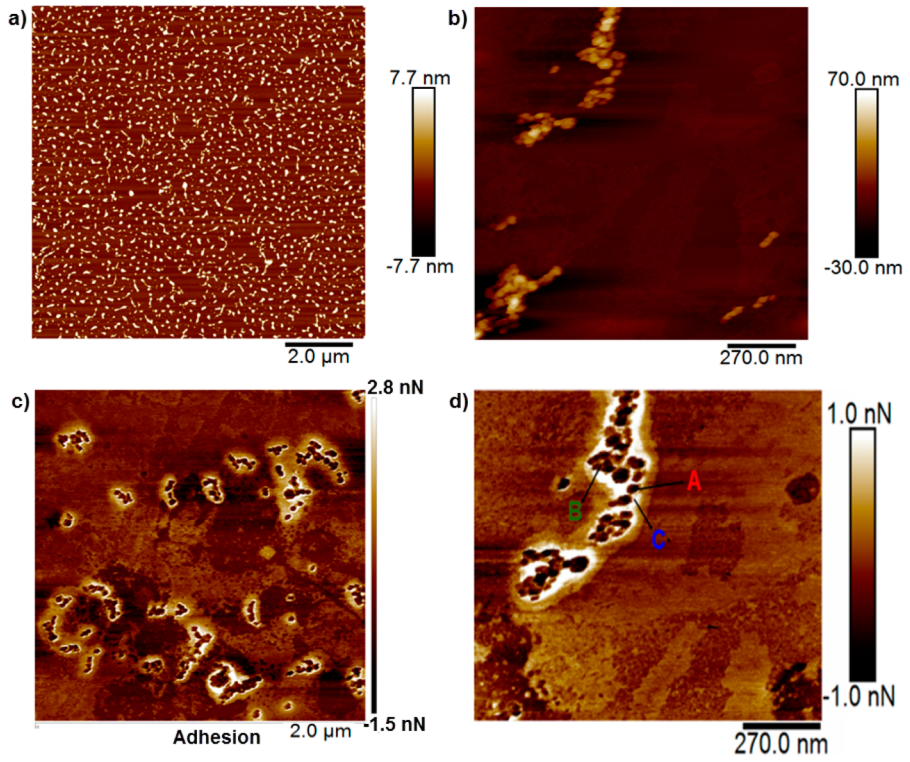

Figure 4. (a) AFM topography image (2 μm scale) of **10**, (b) AFM topography image (270 nm scale) of **AuNSs-10b**, (c) AFM adhesion image (2 μm scale) of **AuNSs-10b**, and (d) AFM adhesion image (270 nm scale) of **AuNSs-10b** where three different regions A, B, and C are represented corresponding to three different force curves (Supporting Information).

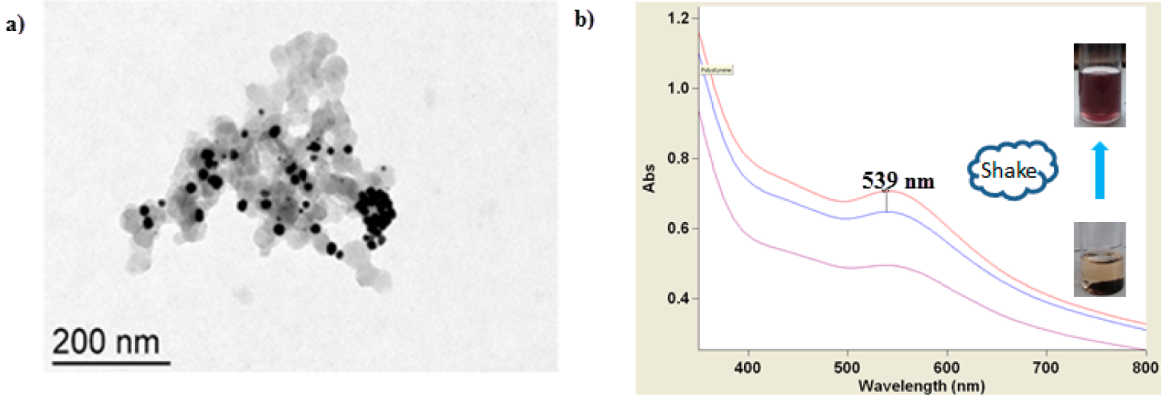

Figure 5. (a) TEM of **AuNPs-14c** and (b) UV−vis spectrum of **14c** (blue line). The violet line corresponds to the UV−vis spectrum after 5 min, and the red line is recorded after shaking of the sample. The photograph shows the flocculated AuNPs and their redissolution by shaking.

Incubation for 1 week of **AuNPs-9a** and **AuNPs-10a** also leads to **AuNSs-9b** and **AuNSs-10b**. TEM analysis of AuNSs-**9b** shows AuNPs of 10.5 ± 1.5 nm (Supporting Information) and TEM analysis of **AuNSs-10b** shows AuNPs of 13.5 ± 1.5 nm (Supporting Information). An isolated vermicular of **AuNSs-10b** presents a thickness of 8.7 ± 1.5 nm and a length of 210 ± 15 nm and encapsulates 11 spherical AuNPs with an inter-nanoparticle distance of 5.2 ± 1.5 nm.

AFM studies were performed on a graphite surface upon peak force tapping. The topography images of polymer **10** show that polymer **10** has an average height of 7 ± 1.5 nm on the graphite surface (Figure 4a). However, the situation changes in the case of **AuNSs-10b.** Long nanosnakes assemblies are observed on the order of 200−300 nm, with a height between 18 and 35 nm (Figure 4b). Peak force tapping mode also permits extraction of qualitative nanomechanical properties. Adhesion of **10b** is mapped and the force curves are recorded. In Figure 4c,d adhesion images recorded at 2 μm and a zoom at one of the nanosnakes at 270 nm respectively provide information on the nature of the nanomaterials. Under the same experimental conditions, in all cases three different force curves are observed corresponding to three different regions. For instance, in Figure 4d, regions A, B, and C give different force curves. Larger adhesion forces are observed in region C (white color) corresponding to an elastic and flexible material that is the organic polymer part. Then, zone A, with the smaller adhesion forces (black color), belongs to a stiffer part of the nanomaterial that corresponds to the AuNPs, and last zone B (brown color) surrounding regions A presents

DOI: 10.1021/ic5028916
Inorg. Chem. 2015, 54, 2284−2299

intermediate force curves due to the electrostatic forces of the trz-BiFc$^+$Cl$^-$ units surrounding the AuNPs.

Even if the polymer structure and length differ, the type of AuNSs is similar in all cases where the trzBiFc units are in the side polymer chain. The role of the incubation time is then examined. TEM analyses of **AuNSs-10b** after 1 and 3 days confirm the need for a 1 week incubation time for the completed formation of these nanostructures. After 1 day, round AuNPs of the same size (13.5 ± 1.5 nm) are formed, whereas after 3 days the reassociation of these nanoparticles is observed even though the nanosnake structure is not yet formed. However, after 1 week of incubation, the association of the polymer-stabilized AuNPs is completed, forming nanosnakes as observed by TEM and AFM microscopies.

Additionally, as expected the role of the polymer/$HAuCl_4$ stoichiometry is crucial. Indeed, for instance upon adding one more equivalent of polymer **10** to $HAuCl_4$ under the same conditions, stable AuNPs of the same size are observed, but after 1 week the formation of nanosnakes does not occur.

In an effort to further confirm the crucial role of the electrostatic interactions of the BiFc$^+$ cations in the formation of the snake-shaped networks and stabilization of AuNPs **AuNSs-14b** was reduced by $NaBH_4$ in DCM/methanol solution. The result is that neutral trzBiFc-stabilized **AuNPs-14c** presents a flocculation phenomenon after 10 min that is taken into account by the absence of electrostatic stabilization. Shaking of the solution redissolves the **AuNPs-14c**, however, and the flocculation phenomenon is fully reversible. The UV−vis spectrum shows the presence of a small shoulder at 450 nm belonging to the trzBiFc and the plasmon band at 539 nm. TEM clearly shows the destruction of the snake-shaped network, whereas the AuNPs remain of the same size (d = 13.5 ± 1.5 nm) (Figure 5).

Besides TEM and UV−vis analysis the **AuNSs-9b**, **AuNSs-10b**, and **AuNSs-14b** are also characterized by IR, near-IR, and CV. IR spectroscopy is an excellent tool to determine whether a mixed-valent complex is electron delocalized or not in the time scale of molecular vibrations. More particularly, the difference of the perpendicular C−H bending vibration is around 815 cm^{-1} for ferrocene, whereas for ferricenium salts it is found around 852 cm^{-1}. For all the AuNSs the IR analysis gives two distinct bands corresponding to the existence of Fe^{II}/Fe^{III}. For example in the case of polymer **14b**, two distinct bands are observed: one at 844 cm^{-1} (corresponding to Fe^{III}) and one at 824 cm^{-1} (corresponding to Fe^{II}) showing localized Fe^{II} and Fe^{III} moieties on the IR time scale. The presence of the Fc$^+$ center close to the Fc group increases the frequency of the Fc side by 9 cm^{-1}, compared to the neutral analogue, polymer **14**. This shift results from the presence of the electron-withdrawing Fc$^+$ substituent (Figure 6).

In order to distinguish between class-I and class-II electron localized mixed valency, the use of near-IR spectroscopy is necessary in order to search the intervalent charge-transfer band that characterizes the optical transition from the ground state to the intervalence charge-transfer state of the class-II mixed-valent compounds. Indeed, the near-IR spectra of all the AuNSs provide the intervalence band (Supporting Information) indicating that the mixed-valent polymers stabilizing the AuNPs belong to class II of mixed-valent compounds.

CV of these AuNSs show both reversible redox waves of the BiFc units, confirming the stability of these nanostructures that also present a strong adsorption phenomenon onto the electrode surface (Supporting Information). However, when

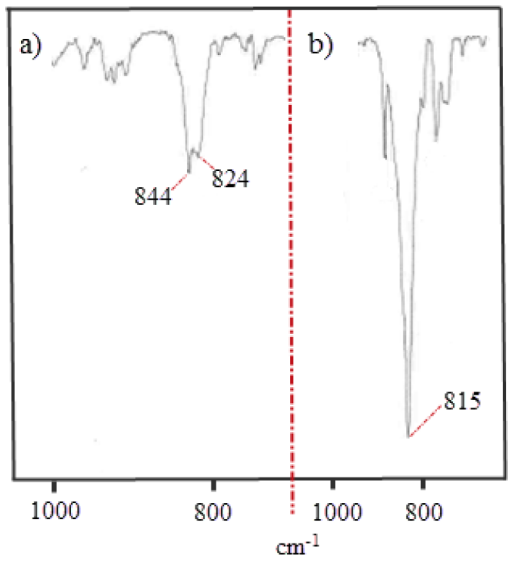

Figure 6. FT-IR (KBr) of (a) mixed-valent biferrocenium-stabilized **AuNSs-14b**, 844 cm^{-1} (ν_{Fc}+) and 824 cm^{-1} (ν_{Fc}), (b) polymer **14**, 815 cm^{-1} (ν_{Fc}).

the same reaction is conducted with polymer **18** in which the trzBiFc$^+$Cl$^-$ units are in main polymer chain, the situation is different (Scheme 7). AuNPs are formed with 12 ± 1 nm size for which surprisingly incubation leads to a well-organized network (AuNN, Figure 7). This is taken into account by the fact that the larger distance between trz-BiFc$^+$ units induces much reduced electrostatic repulsion among the cationic centers that are a key parameter for the nanosnake formation.

A key comparison concerns the possibility of AuNP network formation in the trz-Fc polymers and the non-trz-Fc polymers. The reaction of a trz-Fc-containing poly(norbornene) polymer synthesized by ROMP with $HAuCl_4$ leads to a trz-Fc$^+$ polymer-AuNP species that immediately decomposes owing to the instability of the trz-Fc$^+$ moiety. However, when an amido-Fc ROMP polymer **20**[45] reacts with $HAuCl_4$, small **AuNPs-20a** of 6 ± 1 nm size form, but after 1 week of incubation the TEM analysis does not show the formation of a network (Figure 8).

The trz together with biferrocenium cations are responsible for the organization of the nanomaterials in nanosnakes (when trzBiFc$^+$ are in the side chain) or nanonetworks (when trzBiFc$^+$ are in the main chain).

The method was extended in order to obtain structured silver nanoparticles (AgNPs). Manners et al. have shown the reduction of Ag^I to AgNPs by macromolecules resulting from ferrocenophane ring-opening polymerization.[46] Therefore, we tested the formation of AgNP networks using trzBiFc polymers as reductants under the same conditions as **AuNSs-14b**. Polymer **14** was used to reduce Ag^I stoichiometrically (1:1, trz-BiFc/$AgBF_4$) yielding **AgNPs-21a** in a one-pot reaction. The reduction was immediate as witnessed by the color change from colorless to gray-purple. **AgNPs-21a** are very stable, and after a 4-day incubation time TEM analysis revealed the polymeric vermicular-network formation with a thickness of 36 ± 4 nm in which AgNPs of size d = 4 ± 1 nm are encapsulated (Figure 9). The plasmon band of **AgNSs-21b** was found at λ = 434 nm indicating the formation of the AgNPs, and the ferricenium band was recorded at λ = 600 nm.

The smaller size of the AgNPs found into the polymeric vermicular-shaped network is possibly due to the faster one-

DOI: 10.1021/ic5028916
Inorg. Chem. 2015, 54, 2284−2299

Scheme 7. Synthesis of Gold Nano-Networks AuNNs-18b

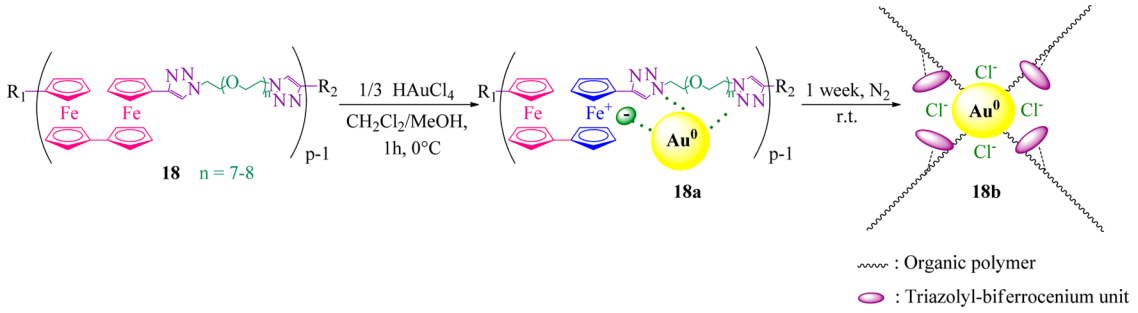

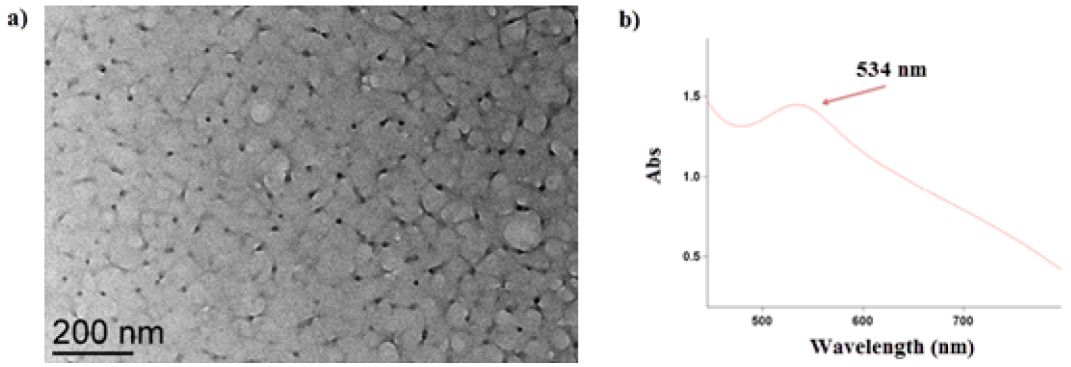

Figure 7. (a) TEM analysis of **AuNNs-18b** at 200 nm, (b) UV–vis spectrum of **AuNNs-18b** peaking at 534 nm (plasmon band).

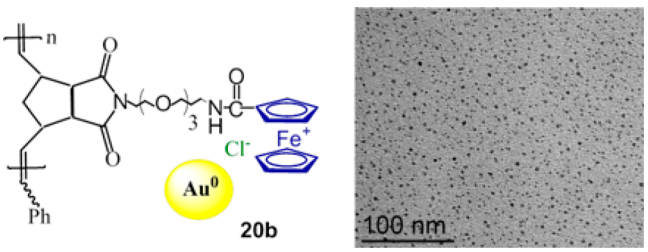

Figure 8. TEM analysis of **20b** at 100 nm.

electron reduction of Ag^{I} compared to the three-electron reduction of Au^{III} under the same conditions. The vermicular-shaped network is formed in both cases **AuNSs-14b** and **AgNSs-21b** confirming that the synergy between the biferrocenium cation, trz ligand coordination, the inter BiFc distance, and the polymer bulk is responsible for this vermicular-shaped network that encapsulates NPs of metals such as gold and silver.

Modified Electrodes and Redox Recognition. Modification of electrodes with polymer films containing reversible redox systems has been successful resulting in detectable electroactive materials.[47] Modified electrodes of polymers **9**, **10**, **14**, and **18** are prepared via absorption by scanning around the BiFc potentials. The electrochemical behavior of these Pt-modified electrodes is first studied in DCM containing only the supporting electrolyte. Two well-defined, symmetrical redox waves are observed in all cases, which is characteristic of surface-confined redox couples, with the expected linear relationship of peak current with potential sweep rate υ (Figure

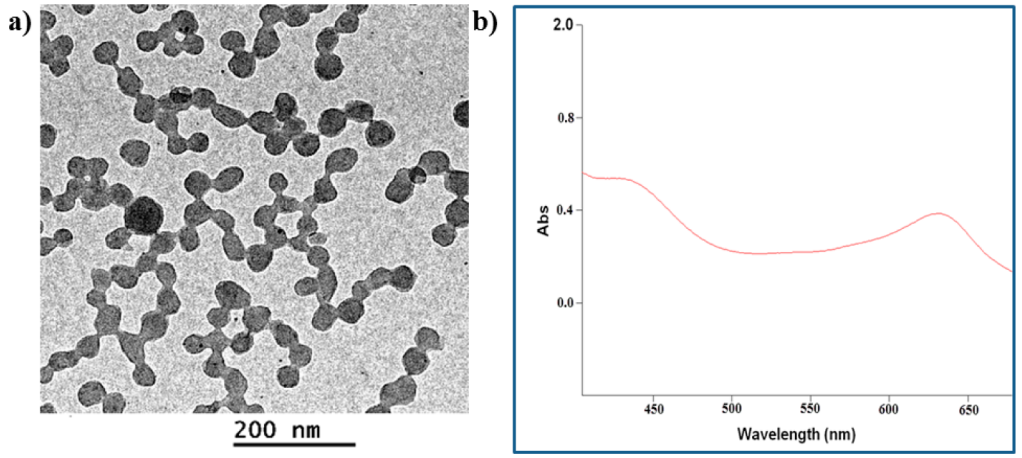

Figure 9. (a) TEM analysis of **AgNSs-21b**, (b) UV–vis spectrum of **AgNSs-21b** showing the plasmon band of AgNPs at λ = 434 nm and the biferrocenium band at λ = 630 nm.

DOI: 10.1021/ic5028916
Inorg. Chem. 2015, 54, 2284–2299

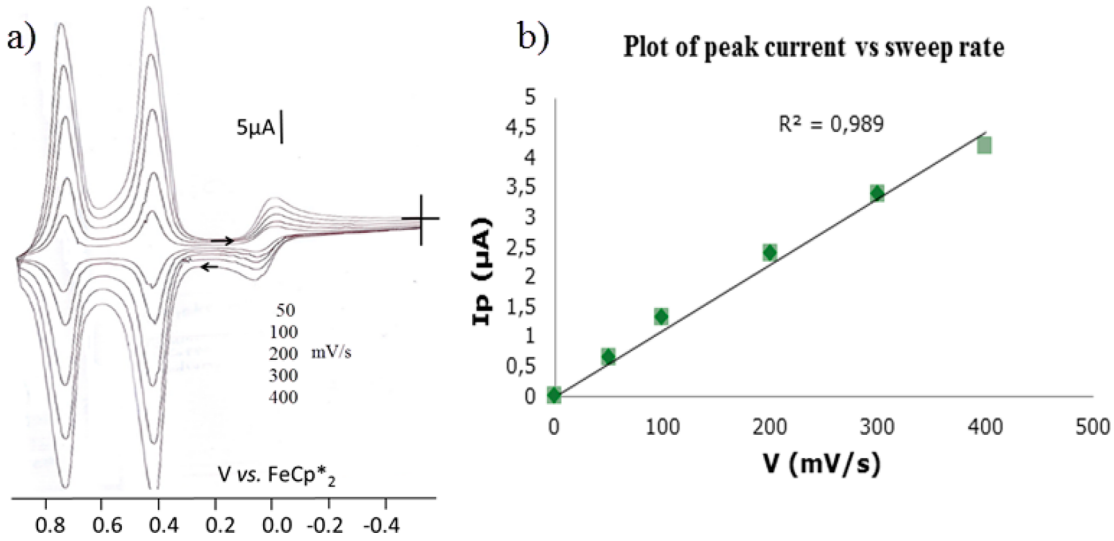

Figure 10. (a) Modified Pt electrode of polymer **14** at various scan rates in a DCM solution containing only 0.1 M $[n\text{-}Bu_4N][PF_6]$ as the supporting electrolyte; (b) intensity as a function of scan rate; linearity shows the expected behavior of an adsorbed polymer.

10b). Repeated scanning does not change the CVs demonstrating that the modified electrodes are stable to electrochemical cycling. However, the stability differs depending on the polymer. The value of the full width at half-maximum (fwhm) for polymers **9**, **10**, **14**, and **18** is measured at a scan rate of 100 mV/s (Table 3). For polymers **9**, **10**, and **14** the

Table 3. Compared Modified Electrodes with Polymers 9, 10, 14, and 18 after 20 ± 5 scans

compound	$\Delta E_{fwhm}{}^a$ (mV)	Γ (mol cm^{-2})^b	$n_d{}^c$
Poly **9**	75	2.1×10^{-10}	3
Poly **10**	72	2.9×10^{-10}	4
Poly **14**	80	3.1×10^{-10}	14
Poly **18**	115	10.4×10^{-10}	1

[a]Values of the full width at half-maximum. [b]Surface coverage of the electroactive BiFc sites of the polymers. [c]Number of days for which the modified electrodes show no loss of electroactivity.

ΔE_{fwhm} are <99/n mV, suggesting the existence of attractive interactions between the BiFc sites attached onto the electrode surface.[48] On the other hand for polymer **18** the ΔE_{fwhm} is 115 mV showing that the biferrocenyl sites have repulsive interactions on the electrode surface (Table 3).

The Pt electrodes that are modified with polymer **14** are the most durable and reproducible ones, as no loss of electroactivity is observed after scanning several times or after standing in air for several days. In Figure 10a the modified electrode is shown with polymer **14** (prepared upon adsorption after 35 cycles around the BiFc potentials) at various scan rates. The intensity as a function of scan rate in Figure 10b shows the expected behavior of an absorbed polymer. The surface coverage of the electroactive biferrocenyl sites of the modified electrode is $\Gamma = 5.3 \times 10^{-10}$ mol cm^{-2}. Consequently, polymer **14** shows the best stability and electroactivity for fabrication of Pt-modified electrodes, and it is further used for redox-recognition studies.

The fabrication of stable modified electrodes in purely aqueous solutions is a step toward redox recognition in water of substrates of biological importance or of water pollutants. Because of its strong polarity, however, water is responsible for the decrease of electrostatic interactions and the unfavorable hydrogen bonding between host and guest molecules. This makes recognition in water much more difficult than in organic solvent. The Pt-modified electrodes that are modified with polymer **14** successfully provide both redox waves of the BiFc units in water. The electrode is first checked in water containing KNO_3 as supporting electrolyte, and both redox waves are observed herewith. The electrochemical reactions of the adjacent BiFc moieties give rise to broad oxidation and reduction CV waves giving a ΔE value for the first wave of 200 mV and the second one of 260 mV, suggesting a very slow heterogeneous electron-transfer process with the electrode surface. However, when NaCl is used as a supporting electrolyte the situation changes. Both waves appear as well-defined, well separated, and chemically and electrochemically reversible under these conditions. The difference between anodic and cathodic peak potentials is superior to 0.0 V, as in such polar media as water the electron transfer becomes slower. Last, the electrode does not lose its electroactivity until at least six successive scans (Figure 11).

*Redox Sensing Using Pt Electrodes Modified with Polymer **14** in Organic Media.* Adenosine triphosphate (ATP) is an

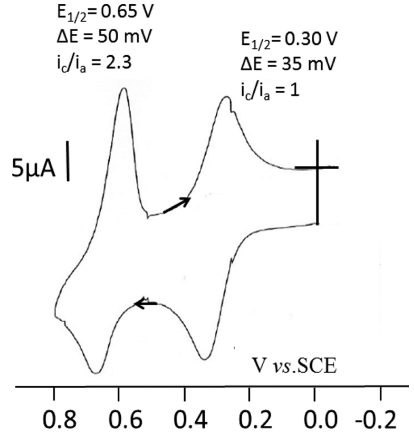

Figure 11. Voltammetric response of a platinum electrode modified with polymer **14**, measured in H_2O/0.1 M NaCl; scan rate: 50 mV s^{-1}.

DOI: 10.1021/ic5028916
Inorg. Chem. 2015, 54, 2284−2299

essential coenzyme that transports chemical energy within cells for the metabolism. A Pt electrode modified with polymer **14** was used for the recognition of ATP in DCM solution containing only $[n\text{-}Bu_4N][PF_6]$ as the supporting electrolyte. Indeed, addition of the adenosyl triphosphate salt $[n\text{-}Bu_4N]_2[ATP]$ provokes a splitting of the outer Fc CV wave at 0.41 V. During titration the new wave is shifted at 120 mV less positive potentials, signifying a rather strong interaction of the outer Fc^+ group with the ATP^{2-} anion, which now makes the oxidation of this Fc group easier than in the absence of ATP. When excess of $[n\text{-}Bu_4N]_2[ATP]$ is added, the initial cathodic wave disapears and is replaced by the new wave (Figure 12). However, electrochemical irreversibility is

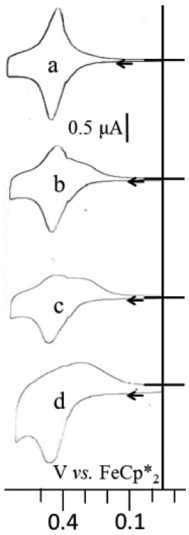

Figure 12. Recognition of ATP^{2-} with a Pt modified electrode with polymer **14**. (a) Modified electrode alone; (b) and (c) in the course of titration (the second wave is not represented as scanning until more positive potentials upon addition of ATP anions provokes instability of the electrode); (d) with an excess of $[n\text{-}Bu_4N]_2[ATP]$. Solvent: DCM; reference electrode: Ag; working and counter electrodes: Pt ; scan rate: 0.3 V/s ; supporting electrolyte: 0.1 M $[nBu_4N][PF_6]$.

observed, which is the sign of a strong structural rearrangement involving supramolecular interactions (hydrogen bonding and electrostatic interactions) in the course of the heterogeneous electron transfer. In comparison, the hexafluorophate salt $[n\text{-}Bu_4N][PF_6]$ does not provoke any CV wave shift.

The most remarkable feature found with trzBiFc-terminated dendrimers[18b] synthesized by CuAAC reaction is the selective recognition in solution of anions by the outer Fc/Fc^+ groups and the recognition of transition-metal cations by the inner Fc/Fc^+ groups. Indeed, in this case, using the Pt electrode modified with polymer **14**, addition of the salt $Pd(OAc)_2$ also provokes the splitting of the wave of the inner Fc group, the new wave appearing at 70 mV more positive potentials. This is due to the coordination of the Pd^{2+} cation to the trz group attached to the inner Fc group and the larger perturbation of this dicationic BiFc group in the presence of another cation such as Pd^{2+} in the electrochemical cell (see Supporting Information, S79). Again in comparison, the addition of the noncoordinating tetra-*n*-butyl ammonium salt $[n\text{-}Bu_4N][PF_6]$ does not provoke any CV wave shift.

Remarkably, modified Pt electrodes made with polymer **14** recognize both cations and anions in a selective way. The outer Fc center recognizes the ATP anion in both DCM and water solutions, and the inner Fc center recognizes the Pd cation.

*Redox Sensing Using Pt Electrodes Modified with Polymer **14** in Aqueous Media.* Recognition of the ATP anion using a Pt-modified electrode with polymer **14** was also attempted in an aqueous medium containing only NaCl as the supporting electrolyte. Upon addition of $[Na]_2[ATP]$ the $E_{1/2}$ of the outer Fc/Fc^+ wave shifts to 30 mV less positive potentials (Supporting Information), a change that is less significant than in organic media, as expected. The ΔE value between the anodic and cathodic potentials for both waves (inner and outer Fc/Fc^+ groups) now becomes much larger (250 mV and 280 mV respectively). This is due to the binding of the ATP anions to the polymer film provoking a strong structural reorganization of the polymer that is attached to the electrode surface and slows down the heterogeneous electron transfer. Last, the intensity of the anodic peak of the second (inner Fc/Fc^+ group) wave decreases in the presence of the ATP anions, indicating strong electrostatic interactions between the cationic biferrocenium groups and the trapped anions. The high electron density around the ferrocenium centers caused by immobilized inserted ATP anions may inhibit the reversible electrochemical response of a fraction of the redox-active groups.

■ CONCLUDING REMARKS

The various syntheses of BiFc-containing polymers (ROMP, radical type, polycondensation), their rich redox activity, and the robustness of the cationic triazolybiferrocenium moiety contrasting with the instability of triazolylferricenium open multiple applications. Au^{III} and Ag^{I} are reduced to Au^0 and Ag^0 respectively by the BiFc units to mixed-valent biferrocenium polymer-stabilized AuNPs respectively, AgNPs in which the remarkable network formation and AuNP encapsulation are controlled by the polymer design, in particular, by the location in the polymer branches or in the polymer main chain of the BiFc units. For instance, with BiFc groups in the side polymer chains, rare interwining snake-shaped polymer networks encapsulating AuNPs are characterized by TEM and AFM. The roles of the trz ligand, electrostatic interactions, and inter-BiFc group distance are crucial in network formation and AuNP and AgNP stabilization. With BiFc groups in the polymer side chains, the outer Fc groups are oxidized at less positive potentials than the inner trzBiFc groups, which allows selective anion (ATP^{2-}) and cation (Pd^{II}) redox recognition in organic solvents using Pt electrodes modified with the polymers, and even to a lesser extent in water despite the strong competition with the supramolecular interactions involving this strongly polar solvent.

■ EXPERIMENTAL SECTION

General Data. See Supporting Information.

Compound 5. *N*-[4-Hydroxybutyl]-*cis*-5-norbornene-exo-2,3-dicarboximide (425 mg, 1.8 mmol) and TsCl (343.6 mg, 1.8 mmol) were dissolved in 30 mL of DCM. Then at 0 °C KOH (403.9 mg, 7.2 mmol) was added in small portions. The mixture was left stirring for 1 h at 0 °C and 10 h at r.t. Then 30 mL of distilled water was added, and the organic phase was separated. The water phase was washed three times with 15 mL of DCM, and the combined organic phases were washed 3 times with 15 mL of water. The organic phase was dried over Na_2SO_4 and filtered. The solvent was evaporated giving product **5** in 90% yield (668 mg). ^1H NMR ($CDCl_3$, 300 MHz), δ_{ppm}: 7.74 and 7.31 (C*H*, 4H of Tos. group), 6.23 (C*H*=C*H*, 2H), 3.97 (CH_2-Tos, 2H), 3.37 (CONCH_2, 2H), 3.20 (C*H*CON, 2H), 2.61 (CH_2CH, 2H), 2.37 (CH_3 of Tos group, 3H), 1.55 ($CH_2CH_2CH_2CH_2$–Tos, 4H),

DOI: 10.1021/ic5028916
Inorg. Chem. 2015, 54, 2284–2299

1.42 and 1.14 (CH_2CH, 2H). ^{13}C NMR ($CDCl_3$, 75 MHz), δ_{ppm}: 177.98 (*C*=O), 144.80 (O*Cq* of Tos. group), 137.87 (CH=*C*H), 132.99 (CH_3*Cq* of Tos. group), 129.91 and 127.96 (*C*H of Tos. group), 69.70 (CH_2-Tos), 47.86 (CH_2CH), 45.25 ($CONCH_2$), 42.74 (CH_2CH), 37.81 (*C*HCON), 26.38 ($CH_2CH_2CH_2CH_2$–Tos), 23.96 ($CH_2CH_2CH_2CH_2$–Tos), 21.55 (CH_3 of Tos. group). ESI MS: Calcd: 412.45, found: 412.12. IR (KBr): 3065 cm^{-1} (=C–H stretching), 1694 cm^{-1} (*C*=O).

Compound 7. *N*-[4-Tosylatebutyl]-*cis*-5-norbornene-*exo*-2,3-dicarboximide **5** (650 mg, 1.6 mmol) was dissolved in 5 mL of DMSO in which NaN_3 (312 mg, 4.8 mmol) was added in small portions. The mixture was left under vigorous stirring at r.t. for 2 days. Then 10 mL of water and 5 mL of DCM were added in the solution. The organic phase was separated, and the water phase was washed 3 times with DCM. The combined organic phase was washed 10 times with 5 mL of water in order to remove all the traces of DMSO. ^1H NMR of *N*-[4-azidobutyl]-*cis*-5-norbornene-*exo*-2,3-dicarboximide **6** ($CDCl_3$, 300 MHz), δ_{ppm}: 6.28 (*CH*=*CH*, 2H), 3.47 (CH_2-N_3, 2H), 3.25 (4H, $CONCH_2$ and *CH*CON), 2.66 (CH_2CH, 2H), 1.59 ($CH_2CH_2CH_2CH_2$– N_3, 4H), 1.48 and 1.16 (CH_2CH, 2H). IR of *N*-[4-azidobutyl]-*cis*-5-norbornene-*exo*-2,3-dicarboximide (KBr): 3065 cm^{-1} (=C–H stretching), 2097 cm^{-1} (-N_3), 1698 cm^{-1} (*C*=O). *N*-[4-Azidobutyl]-*cis*-5-norbornene-*exo*-2,3-dicarboximide **6** (200 mg, 0.76 mmol) and compound **3**[2] (359.4 mg, 0.91 mmol) were dissolved in 20 mL of distilled THF. Then 3 mL of degassed water was added into the solution, and the reaction mixture was cooled to 0 °C. Then, an aqueous solution of $CuSO_4$ 1 M (1.1 equiv) was added dropwise, followed by the dropwise addition of a freshly prepared solution of sodium ascorbate (2.2 equiv). The color of the solution changed from orange to dark red upon addition of sodium ascorbate. The reaction mixture was allowed to stir for 16 h at r.t. under nitrogen atmosphere. Then, the mixture of solvents was evaporated *in vacuo*, and 100 mL of DCM was added, followed by the addition of an aqueous solution of ammonia. The mixture was allowed to stir for 15 min in order to remove the copper salt. The organic phase was washed twice with water, dried over sodium sulfate, and filtered and the solvent was removed *in vacuo*. Then the product was precipitated twice from a DCM solution in pentane. Product **7** was obtained as an orange crystalline powder. Yield: 97% (488 mg). ^1H NMR ($CDCl_3$, 300 MHz), δ_{ppm}: 7.03 (trz, 1H), 6.26 (*CH*=*CH*, 2H), 4.50 (CH_2-trz, 2H), 4.21, 4.14, 4.10, 4.06, (Cp sub., 12H), 3.90 (Cp free, 5H), 3.49 (2H, $CONCH_2$), 3.25 (2H, *CH*CON), 2.66 (CH_2CH, 2H), 1.53 ($CH_2CH_2CH_2CH_2$–trz, 4H), 1.47 and 1.18 (CH_2CH, 2H). ^{13}C NMR ($CDCl_3$, 75 MHz), δ_{ppm}: 177.96 (*C*=O), 145.33 (*Cq* of trz), 137.75 (CH=*C*H), 119.36 (*C*H of trz), 85.39, 83.46, and 72.92 (*Cq* of BiFc), 69.38, 69.19, 68.94, 67.51, 67.09, 66.10 (*C*H of BiFc) 47.85 (CH_2CH), 45.13 ($CONCH_2$), 42.74 (CH_2CH), 37.61 (*C*HCON), 27.43 ($CH_2CH_2CH_2CH_2$–trz), 24.81 ($CH_2CH_2CH_2CH_2$–trz). IR (KBr): 3090 cm^{-1} (=C–H stretching), 1698 cm^{-1} (*C*=O), 815 cm^{-1} (Fe^{II}). ESI MS: Calcd: 654.35, found: 654.14. UV–vis: λ_{max} = 450 nm, ε_o = 500.4 L.cm^{-1} mol^{-1}. Anal. Calcd for $C_{35}H_{34}N_4O_2Fe_2$: C, 64.25; H, 5.24. Found: C, 64.12; H, 4.98.

Polymer 9. Compound **7** (60 mg, 0.09 mmol) was added into a small Schlenk flask that was flushed with nitrogen and dissolved in 0.2 mL of dry DCM. Then, catalyst **8** (2.6 mg, 0.003 mmol) in 0.1 mL of dry DCM was quickly added into the monomer solution under nitrogen atmosphere with vigorous stirring. The reaction mixture was vigorously stirred for 5 h, and then quenched with 0.2 mL ethyl vinyl ether (EVE). The orange solid polymer **9** was purified by precipitation in methanol twice and dried *in vacuo* (57 mg, 98% yield). ^1H NMR (CD_2Cl_2, 400 MHz), δ_{ppm}: 7.22 and 7.16 (*C*H of trz), 5.75 and 5.55 (*CH*=*CH*, 2H), 4.60 (CH_2-trz, 2H), 4.30, 4.28, 4.19 (Cp sub. of BiFc), 3.98 (Cp free of BiFc), 3.49 ($CONCH_2$, 2H), 3.04 (*CH*CON, 2H), 2.69 and 2.09 (CH_2CH, 2H), 1.86 and 1.61 ($CH_2CH_2CH_2CH_2$–trz, 4H) and (CH_2CH, 2H). ^{13}C NMR (CD_2Cl_2, 75 MHz), δ_{ppm}: 178.39 (*C*=O), 145.31 (*Cq* of trz), 133.50 and 132.07 (*CH*=*CH*), 119.85 (*C*H of trz), 85.73, 83.02, 77.06, 70.98 (*Cq* of Cp of BiFc), 70.98, 69.57 (*C*H of Cp free of BiFc) 69.35, 67.84, 67.47, 66.53 (*C*H of Cp sub. of BiFc), 49.59 (CH_2CH), 46.39 ($CONCH_2$), 42.97 (CH_2CH), 37.90 (*C*HCON), 26.33 ($CH_2CH_2CH_2CH_2$–trz), 26.29 (CH_2-trz), 25.11 ($CH_2CH_2CH_2CH_2$–trz). IR (KBr): 3090 cm^{-1} (=C–H stretching), 1698 cm^{-1} (*C*=O), 816 cm^{-1} (Fe^{II}). UV–vis: λ_{max} = 450 nm, ε = 15673,7 L.cm^{-1} mol^{-1}. MALDI-TOF MS for $C_6H_6(C_{37}H_{36}N_4O_2Fe_2)_3C_2H_2Na$: Calcd: 2168.3, Found: 2168.5. SEC: PDI = 1.23. Dynamic light scattering (DLS): d = 14.3 ± 3 nm.

Polymer 10. Compound **7** (60 mg, 0.09 mmol) was added into a small Schlenk flask that was flushed with nitrogen and dissolved in 0.2 mL of dry DCM. Then, catalyst **8** (1.3 mg, 0.002 mmol) in 0.1 mL of dry DCM was quickly added into the monomer solution under nitrogen atmosphere with vigorous stirring that was continued for 5 h. The catalyst was quenched with 0.2 mL of EVE, and the orange solid polymer **10** was purified by precipitation in methanol twice and dried *in vacuo* (58 mg, 99% yield). ^1H NMR (CD_2Cl_2, 400 MHz), δ_{ppm}: 7.21 and 7.13 (*C*H of trz), 5.72 and 5.53 (*CH*=*CH*, 2H), 4.55 (CH_2-trz, 2H), 4.28, 4.27, 4.16 (Cp sub. of BiFc), 3.94 (Cp free of BiFc), 3.45 ($CONCH_2$, 2H), 3.00 (*CH*CON, 2H), 2.67 and 2.06 (CH_2CH, 2H), 1.82 and 1.56 ($CH_2CH_2CH_2CH_2$–trz, 4H) and (CH_2CH, 2H). ^{13}C NMR (CD_2Cl_2, 75 MHz), δ_{ppm}: 178.22 (*C*=O), 145.14 (*Cq* of trz), 133.38 and 131.94 (*CH*=*CH*), 119.58 (*C*H of trz), 85.08, 82.99, 76.72, 70.00 (*Cq* of Cp of BiFc), 69.39, 69.20 (*C*H of Cp free of BiFc) 68.99, 67.57, 67.34, 66.37 (*C*H of Cp sub. of BiFc), 49.32 (CH_2CH), 46.03 ($CONCH_2$), 45.87 (CH_2CH), 37.59 (*C*HCON), 29.69 ($CH_2CH_2CH_2CH_2$–trz), 27.42 (CH_2-trz), 24.71 ($CH_2CH_2CH_2CH_2$–trz). IR (KBr): 3091 cm^{-1} (=C–H stretching), 1698 cm^{-1} (*C*=O), 816 cm^{-1} (Fe^{II}). . UV–vis: λ_{max} = 450 nm, ε = 26 470 L·cm^{-1} mol^{-1}. SEC: PDI = 1.21. DLS: d = 36.9 ± 7 nm;

Polymer 14. Azidomethylpolystyrene (13.4 mg, 0.084 mmol, 1 equiv) and ethynylbiferrocene **3** (36.0 mg, 0.091 mmol, 1.1 equiv) were dissolved in distilled toluene under nitrogen. Then, 15% of the catalyst **13**, [Cu^Itren($CH_2Ph)_6$][Br], (11 mg, 0.013 mmol, 0.15 equiv) was added. The mixture was left for 16 h at 50 °C. The orange precipitate that was formed was washed twice with hot toluene and solubilized in DCM. Evaporation of the solvent *in vacuo* gave the polytriazolyl(biferrocenyl) methylstyrene **14** as an orange waxy product (45 mg, 97% yield). ^1H NMR (THF-d_8, 300 MHz) δ_{ppm}: 6.92 (*C*H of trz), 6.82, 6.32 (4H, *C*H of Ar of styrenyl), 5.41 (2H, CH_2-triazole), 4.71, 4.32, 4.16 (12H of Cp sub. BiFc), 3.92 (5H of Cp BiFc), 1.62, 1.16 (*C*H and CH_2 of polymer chain). ^{13}C NMR (THF-d_8, 75 MHz) $\delta_{ppm:}$ 145.00 (*Cq* of trz), 144.40 (*Cq* of Ar), 133.68 (*Cq*-CH_2 of Ar), 127.82 and 127.39 (*C*H of Ar), 120.76 (*C*H of trz) 85.36, 82.55, 77.57 (*Cq* of Cp sub. of BiFc), 69.77, 69.20, 68.96, and 67.57 (*C*H of BiFc), 52.92 (CH_2-trz), 40.21 (*C*H and CH_2 of polymeric chain). SEC: PDI = 1.25. DLS: d = 11.9 ± 2 nm. IR (KBr): 3092 cm^{-1} (=C–H vibration of Cp and trz) and 815 cm^{-1} (Fe^{II}). UV–vis: λ_{max} = 455 nm, ε = 14896.6 L·cm^{-1} mol^{-1}.

Polymer 18. 1.665×10^{-4} mol of **15** (74.9 mg, M_w = 450 g·mol^{-1}) and the same molar quantity of **17** (69.9 mg, M_w = 418 g·mol^{-1}) were introduced into a Schlenk flask with 2.8 mL of THF under nitrogen. Then 3.33×10^{-4} mol of $CuSO_4$, $5H_2O$ (53.24 mg) were solubilized in 1.8 mL of water and added in the reaction medium, and 6.66×10^{-4} mol of NaAsc (131.84 mg) was solubilized in 1 mL of water and added dropwise to the reaction medium. The reaction was stirred at 40 °C during 2 days, and an orange precipitate was observed on the wall of the Schlenk flask. Then 1 mL of an ammonia solution (37% mol) was added together with 5 mL of H_2O and 5 mL of DCM. The solution was stirred for 5 min, the organic phase was recovered, and the aqueous phase was washed twice with 5 mL of DCM. The combined organic phase was gathered, washed with H_2O (3 × 5 mL), and dried with Na_2SO_4. After concentration of the organic phase (1 mL), the polymer was precipitated twice in 60 mL of Et_2O. Then 113 mg of **18** were obtained (78% yield) as an orange solid film polymer. ^1H NMR ($CDCl_3$, 400 MHz) δ_{ppm}: 7.23 (2H, *C*H of trz), 4.48 (4H, Cp sub.), 4.43 (4H, $-CH_2$trz), 4.09 (4H, Cp sub.), 4.04 (8H, Cp sub.), 3.83 (4H, -OCH_2CH_2trz), 3.57–3.60 ($-OCH_2CH_2O$ of PEG_{400}). ^{13}C NMR (CDCl3, 100 MHz), δ_{ppm}: 145.2 (*Cq* of trz), 120.6 (*C*H of trz), 83.9 and 77.0 (*Cq* of Cp sub.), 70.7 (-OCH_2CH_2O of PEG_{400}), 69.7 and 69.6 (*C*H of Cp sub.), 68.9 (-OCH_2CH_2trz), 67.7 and 67.4 (*C*H of Cp sub.), 50.2 ($-OCH_2CH_2$trz). IR (KBr): 3121 cm^{-1} (=C–H vibration of Cp and trz) 1110 (C–O) and 819 cm^{-1} (Fe^{II}).

DOI: 10.1021/ic5028916
Inorg. Chem. 2015, 54, 2284–2299

Polymer 19. 1.196 × 10^{-4} mol of **16** (125.8 mg, M_w = 1052 g·mol^{-1}) and the same molar quantity of **17** (50 mg, M_w = 418 g·mol^{-1}) were introduced under nitrogen into a Schlenk flask together with 3 mL of THF. Then 1.53 × 10^{-4} mol of $CuSO_4$, $5H_2O$ (38 mg) were solubilized in 1 mL of water and added in the reaction medium, and 4.75 × 10^{-4} mol of NaAsc (94 mg) was solubilized in 1 mL of water and added dropwise to the reaction medium. The reaction was stirred at 40 °C during 2 days, and an orange precipitate was observed on the wall of the Schlenk flask. Then 1 mL of an ammonia solution (37% mol) was added together with 5 mL of H_2O and 5 mL of DCM. The solution was stirred during 5 min, then the organic phase was recovered, and the aqueous phase was washed twice with 5 mL of DCM. The organic phases were gathered, washed with H_2O (3 × 5 mL), and dried over Na_2SO_4. After concentration of the organic phase (1 mL), the polymer was precipitated in 60 mL of Et_2O, and 62.5 mg was obtained as an orange-red paste (58% yield). ^{1}H NMR ($CDCl_3$, 200 MHz) δ_{ppm}: 7.25 (2H, C*H* of trz), 4.54 (4H, Cp sub.), 4.44 (4H, −CH_2trz), 4.11 (8H, Cp sub.), 4.08 (4H, Cp sub.), 3.84 (4H, OCH_2CH_2trz), 3.61−3.65 (−OCH_2CH_2O of PEG_{400}). ^{13}C NMR ($CDCl_3$, 100 MHz), δ_{ppm}: 145.1 (*Cq* of trz), 120.5 (*C*H of trz), 83.9 and 76.3 (*Cq* of Cp sub.), 70.5 (-OCH_2CH_2O of PEG_{400}), 69.4 and 69.3(CH of Cp sub.), 68.7 (-OCH_2CH_2trz), 67.4 and 67.2 (*C*H of Cp sub.), 50.2. IR (KBr): 3092 cm^{-1} (=C−H vibration of Cp and trz), 1109 (C−O) and 819 cm^{-1} (Fe^{II}).

AuNSs-9b. Polymer **9** [10 mg, 0.015 mmol (M_w monomer: 654 g·mol^{-1}), 1 equiv] was dissolved in 1 mL of DCM and added dropwise at 0 °C into a stirring solution of $HAuCl_4·3H_2O$ (2.0 mg, 0.005 mmol, 1/3 equiv) in 4 mL of methanol/DCM 3:1. The color immediately changed from orange to deep green, stirring continued for another 30 min, and then the mixture was concentrated *in vacuo* to 3 mL and kept in a closed Schlenk tube for 1 week (incubation time) giving compound **9b**. IR (KBr): 3098 cm^{-1} (=C−H vibration of Cp and trz), 834 cm^{-1} (Fe^{III}) and 813 cm^{-1} (Fe^{II}). UV−vis: λ_{max} = 535 nm. TEM: 10.5 ± 1.5 nm.

AuNSs-10b. Polymer **10** [10 mg, 0.015 mmol (M_w monomer: 654 g·mol^{-1}), 1 equiv] was dissolved in 1 mL of DCM and was added dropwise at 0 °C in a stirring solution of $HAuCl_4$ (2.0 mg, 0.005 mmol, 1/3 equiv) in 4 mL of methanol/DCM 3:1. The color instantaneously changed from orange to deep green, and stirring was continued for another 30 min. The mixture was concentrated *in vacuo* to 3 mL and kept in a closed Schlenk tube for 1 week (incubation time) giving compound **10b**. IR (KBr): 3087 cm^{-1} (=C−H vibration of Cp and trz), 834 cm^{-1} (Fe^{III}), and 815 cm^{-1} (Fe^{II}). UV−vis: λ_{max} = 537 nm. TEM: 13.5 ± 1.5 nm.

AuNSs-14b. Polymer **14** [10 mg, 0.018 mmol (monomer M_w: 553 g·mol^{-1}), 1 equiv] was dissolved in 1 mL of DCM and was added dropwise, at 0 °C in a stirring solution of $HAuCl_4$ (2.4 mg, 0.006 mmol, 1/3 equiv) in 4 mL of methanol/DCM 3:1. The color changed instantaneously from orange to deep green, and stirring was continued for another 30 min. The mixture was concentrated *in vacuo* to 3 mL and kept in a closed Schlenk tube for 1 week (incubation time) giving compound **14b**. IR (KBr): 3093 cm^{-1} (=C−H vibration of Cp and trz), 844 cm^{-1} (Fe^{III}), and 824 cm^{-1} (Fe^{II}). UV−vis: λ_{max} = 531 nm. TEM: 13.5 ± 1.5 nm.

AuNPs-14c. To the above solution of **14b** was added 3 mL of CH_2Cl_2. Then under N_2 and vigorous stirring a solution of $NaBH_4$ (1 mg, 0.027 mmol) in 2 mL of methanol was added dropwise. The color immediately changed from green to deep red. The solution was stirred for an additional 5 min, and then the product was immediately filtered. The compound **14c** precipitated (flocculation) in 10 min, but it is again redissolved upon shaking, and this process is reversible. UV−vis: λ_{max} = 539 nm. TEM: 13.5 ± 1.5 nm.

AuNNs-18b. Polymer **18** [10 mg, 0.012 mmol (monomer M_w: 868 g·mol^{-1}), 1 equiv] was dissolved in 1 mL of DCM and added dropwise at 0 °C into a stirring solution of $HAuCl_4$ (1.5 mg, 0.004 mmol, 1/3 equiv) in 4 mL of methanol/DCM 3:1. The color instantaneously changed from orange to deep green, and stirring continued for another 30 min. The mixture was concentrated *in vacuo* to 3 mL and kept in a closed Schlenk tube for 1 week (incubation time) giving compound **18b**. IR (KBr): 3087 cm^{-1} (=C−H vibration of Cp and trz), 834 cm^{-1} (Fe^{III}) and 815 cm^{-1} (Fe^{II}). UV−vis: λ_{max} = 534 nm. TEM: 12.0 ± 1 nm.

AuNPs-20b. Polymer **20** [10 mg, 0.018 mmol (monomer M_w: 550 g·mol^{-1}), 1 equiv] was dissolved in 1 mL of DCM and added dropwise at 0 °C into a stirring solution of $HAuCl_4$ (2.4 mg, 0.006 mmol, 1/3 equiv) in 4 mL of methanol/DCM 3:1. The color changed instantaneously from orange to deep green, and stirring continued for another 30 min. The mixture was concentrated by vacuum to 3 mL and kept in a closed Schlenk tube for 1 week (incubation time) giving compound **20b**. UV−vis: λ_{max} = 528 nm. TEM: 6 ± 1 nm.

AgNSs-21b. Polymer **14** [10 mg, 0.018 mmol (monomer M_w: 553 g·mol^{-1}), 1 equiv] was dissolved in 1 mL of DCM and added dropwise at 0 °C in a stirring solution of $AgBF_4$ (3.5 mg, 0.018 mmol, 1 equiv) in 4 mL of methanol/DCM 3:1. The color instantaneously changed from orange to gray-purple, and stirring was continued for another 30 min. The mixture was concentrated *in vacuo* to 3 mL and kept in a closed Schlenk tube for 1 week (incubation time) giving compound **21b**. IR (KBr): 818 cm^{-1} (Fe^{III}) and 808 cm^{-1} (Fe^{II}). UV−vis: λ_{max} = 434 nm. TEM: 4 ± 1 nm.

CV Measurements. All electrochemical measurements were recorded under nitrogen atmosphere. Solvent: dry DCM; temperature: 20 °C; supporting electrolyte: [*n*-Bu_4N][PF_6] 0.1 M; working and counter electrodes: Pt; reference electrode: Ag; internal reference: $FeCp^*_2$; scan rate: 0.200 V·s^{-1}. The number of electrons involved in the oxidation wave of the BiFc polymers was calculated using Bard's equation: $n_p = (i_{dp}/C_p)/(i_{dm}/C_m)(M_p/M_m)^{0.275}$ (see text).[42] The experiments were conducted by adding a known amount of each polymer in 3 mL of dry DCM and a known amount of $FeCp^*_2$ in 2 mL of DCM. After the CVs were recorded, the intensities of the oxidation waves of the polymers and of the internal reference ($FeCp^*_2$) were measured. The values were introduced in the above equation giving the final number of electrons (n_e). The compared modified electrodes were prepared by approximately 20 adsorption cycles around the BiFc potentials on Pt electrodes. Their electrochemical behavior was checked in 5 mL DCM solution containing only [*n*-Bu_4N][PF_6] 0.1 M at various scan rates: 25, 50, 100, 200, 300, 400, 500, and 600 mV/s. The modified electrodes used for redox recognition were prepared using approximately 35 adsorption cycles around the BiFc potentials on Pt electrodes. Their electrochemical behavior was checked in 5 mL DCM solution containing only [*n*-Bu_4N][PF_6] 0.1 M at various scan rates: 25, 50, 100, 200, 300, 400, 500, and 600 mV/s and in 5 mL H_2O solution containing only [NaCl] 0.1 M. Redox recognition was conducted in two different ways: (a) the CVs were recorded upon addition of [*n*-Bu_4N]$_2$[ATP] or $Pd(OAc)_2$ to an electrochemical cell containing a Pt modified electrode in DCM and (b) the CVs were recorded upon addition of $[Na]_2$[ATP] to an electrochemical cell containing a Pt modified electrode in water.

■ ASSOCIATED CONTENT

Ⓢ Supporting Information

Spectroscopic data for all the complexes and NMR, IR, near-IR, UV−vis. spectra and CVs. This material is available free of charge via the Internet at http://pubs.acs.org.

■ AUTHOR INFORMATION

Corresponding Author

*E-mail: d.astruc@ism.u-bordeaux1.fr.

Notes

The authors declare no competing financial interest.

■ ACKNOWLEDGMENTS

Helpful assistance and discussion with Jean-Michel Lanier (NMR) and Claire Mouche (MALDI-TOF MS) from the CESAMO and Dr. Roberto Ciganda (Université de Bordeaux), and financial support from the Université de Bordeaux, the Centre National de la Recherche Scientifique (CNRS), the

DOI: 10.1021/ic5028916
Inorg. Chem. 2015, 54, 2284−2299

Agence Nationale pour la Recherche (ANR) and L'Oréal are gratefully acknowledged.

REFERENCES

(1) (a) Page, J. A.; Wilkinson, G. *J. Am. Chem. Soc.* **1952**, *74*, 6149−6150. (b) Nishihara, H. *Adv. Inorg. Chem.* **2002**, *53*, 41−86. (c) Geiger, W. E. *Organometallics* **2007**, *26*, 5738−5765. (d) Geiger, W. E. *Organometallics* **2011**, *30*, 28−31.

(2) (a) Connelly, N. G.; Geiger, W. E. *Adv. Organomet. Chem.* **1984**, *23*, 1−93. (b) Connelly, N. G.; Geiger, W. E. *Chem. Rev.* **1996**, *96*, 877−910. (c) Madonik, A. M.; Astruc, D. *J. Am. Chem. Soc.* **1984**, *106*, 2437−2439. (d) Lacoste, M.; Varret, F.; Toupet, L.; Astruc, D. *J. Am. Chem. Soc.* **1987**, *109*, 6504−6506. (e) Desbois, M.-H.; Astruc, D.; Guillin, J.; Varret, F.; Trautwein, A. X.; Villeneuve, G. *J. Am. Chem. Soc.* **1989**, *111*, 5800−5809.

(3) (a) Hamon, J.-R.; Astruc, D.; Michaud, P. *J. Am. Chem. Soc.* **1981**, *103*, 758−766. (b) Green, J. C.; Kelly, M. R.; Payne, M. P.; Seddon, E. A.; Astruc, D.; Hamon, J.-R.; Michaud, P. *Organometallics* **1983**, *2*, 211−218.

(4) (a) Gagne, R. R.; Koval, C. A.; Licensky, G. C. *Inorg. Chem.* **1980**, *19*, 2854−2855. (b) Krejic, M.; Danek, M.; Hartl, F. *J. Electroanal. Chem.* **1991**, *317*, 179−187. (c) Menon, V. P.; Martin, C. R. *Anal. Chem.* **1995**, *67*, 1920−1928. (d) Losada, J.; Cuadrado, I.; Moran, M.; Casado, C. M.; Alonso, B.; Barranco, M. *Anal. Chim. Acta* **1997**, *338*, 191−198. (e) Daeneke, T.; Kwon, T. H.; Holmes, A. B.; Duffy, N. W.; Bach, U.; Spiccia, L. *Nat. Chem.* **2011**, *3*, 211−215.

(5) (a) Wakatsuki, Y.; Yamazaki, H. *Synthesis* **1976**, *1*, 26−28. (b) Astruc, D. *Nat. Chem.* **2012**, *4*, 255−267. (c) Foo, C.; Sella, E.; Thomé, I.; Eastgate, M. D.; Baran, P. S. *J. Am. Chem. Soc.* **2014**, *136*, 5279−5282.

(6) (a) Top, S.; Dauer, B.; Vaissermann, J.; Jaouen, G. *J. Organomet. Chem.* **1997**, *541*, 355−361. (b) Van Staveren, D. R.; Metzler-Nolte, N. *Chem. Rev.* **2004**, *104*, 5931−5985. (c) Ornelas, C. *New J. Chem.* **2011**, *35*, 1973−1985. (d) Gasser, G.; Ott, I.; Metzler-Nolte, N. *J. Med. Chem.* **2011**, *54*, 3−25. (e) Pigeon, P.; Gormen, M.; Kowalski, K.; Muller-Bunz, H.; McGlinchey, M. J.; Top, S.; Jaouen, G. *Molecules* **2014**, *19*, 10350−10369. (f) Matschke, M.; Alborzinia, A.; Lieb, M.; Metzler-Nolte, N. *ChemMedChem* **2014**, *9*, 1188−1194.

(7) (a) Cass, A. E. G; Davis, G.; Francis, G. D.; Hill, H. A. O.; Aston, W. J.; Giggins, I. J.; Plotkin, E. V.; Scott, L. D. L.; Turner, A. P. F. *Anal. Chem.* **1984**, *56*, 667−671. (b) Beer, P. D. *Acc. Chem. Res.* **1998**, *31*, 71−80. (c) Casado, C. M.; Cuadrado, I.; Moran, M.; Alonso, B.; Garcia, B.; Gonzales, B.; Losada, J. *Coord. Chem. Rev.* **1999**, *185−6*, 53−79. (d) Beer, P. D.; Gale, P. A. *Angew. Chem., Int. Ed.* **2001**, *40*, 486−516. (e) Casado, C. M.; Alonso, B.; Losada, J. ; Garcia-Armada, M. P. In *Designing Dendrimers*; Campagna, S., Ceroni, P., Punteriero, F., Eds.; Wiley: Hoboken, NJ, USA, 2012; pp 219−262. (f) Jimenez, A.; Armada, M. P. G.; Losada, L.; Villena, C.; AloAnso, B.; Casado, M. *Sensors Actuators B-Chem.* **2014**, *190*, 111−119.

(8) (a) Nguyen, P.; Gomez-Elipe, P.; Manners, I. *Chem. Rev.* **1999**, *99*, 1515−1548. (b) Abd-El-Aziz, A. S.; Bernardin, S. *Coord. Chem. Rev.* **2000**, *203*, 219−267. (c) Abd-El-Aziz, A. S.; Todd, E. K. *Coord. Chem. Rev.* **2003**, *246*, 3−52. (d) *Macromolecules Containing Metal and Metal-Like Elements, Organoiron Polymers*, Vol 2, Eds: Abd-El-Aziz, A. S.; Carraher Jr., C. E.; Pittman Jr., C. U.; Sheats, J. E.; Zeldin, M.; Wiley-Interscience: Hoboken: NJ, 2003. (e) Abd-El-Aziz, A. S.; Manners, I. *J. Inorg. Organomet. Polym.* **2005**, *15*, 157−195. (f) *Frontiers in Transition-Metal Containing Polymers*, A. S. Abd-El-Aziz, Manners, I., Eds.; Wiley: New York, 2007. (g) Martinez, F. J.; Gonzalez, B.; Alonso, B.; Losada, J.; Garcia-Armada, M. P.; Casado, C. M. *J. Inorg. Organomet. Polym. Mater.* **2008**, *18*, 51−58.

(9) (a) Manners, I. *Science* **2001**, *294*, 1664−1666. (b) Whittel, G. R.; Manners, I. *Adv. Mater.* **2007**, *19*, 3439−3468. (c) Hudson, Z.; Boot, C. E.; Robinson, M. E.; Rupar, P. A.; Winnink, M. A.; Manners, I. *Nat. Chem.* **2014**, *6*, 893−898.

(10) (a) Abakumova, L. G.; Abakumov, G. A.; Razuvaev, G. A. *Dokl. Akad. Nauk SSSR* **1975**, *220*, 1317−1320. (b) Huang, W. H.; Jwo, J. J. *J. Chin, Chem. Soc.* **1991**, *38*, 343−350. (c) Zotti, G.; Schiavon, G.; Zecchin, S.; Berlin, A.; Pagani, G. *Langmuir* **1998**, *14*, 1728−1733. (d) Hurvois, J.-P.; Moinet, C. *J. Organomet. Chem.* **2005**, *690*, 1829−1839.

(11) (a) Cowan, D. O.; Kaufman, F. *J. Am. Chem. Soc.* **1970**, *92*, 219−220. (b) Cowan, D. O.; Kaufman, F. *J. Am. Chem. Soc.* **1971**, *93*, 3889−3893. (c) Levanda, C.; Cowan, D. O.; Bechgaard, K. *J. Am. Chem. Soc.* **1975**, *97*, 1980−1981. (d) Power, M. J.; Meyer, T. J. *J. Am. Chem. Soc.* **1978**, *100*, 4393−4398.

(12) (a) Robin, M. B.; Melvin, B.; Day, P. *Adv. Inorg. Chem. Radiochem.* **1967**, *10*, 247−403. (b) Allen, G. C.; Hush, N. S. *Prog. Inorg. Chem.* **1967**, *8*, 357−390. (c) Richardson, D. E.; Taube, H. *Coord. Chem. Rev.* **1984**, *60*, 107−129.

(13) (a) Horikoshi, T.; Itoh, M.; Kurihara, M.; Kubo, K.; Nishihara, H. J. *Electroanal. Chem.* **1999**, *473*, 113−116. (b) Nishihara, H. *Bull. Soc. Chem. Jpn.* **2001**, *74*, 19−29. (c) Yamada, M.; Nishihara, H. *Chem. Commun.* **2002**, 2578−2579. (d) Yamada, M.; Nishihara, H. *Eur. Phys. J.* **2003**, *24*, 257−260. (e) Yamada, M.; Nishihara, H. *Langmuir* **2003**, *19*, 8050−8056. (f) Yamada, M.; Nishihara, H. *ChemPhysChem* **2004**, *5*, 555−559. (g) Yamada, M.; Tadera, T.; Kubo, K.; Nishihara, H. *J. Phys. Chem. B* **2003**, *107*, 3703−3711. (h) Muraa, M.; Nishihara, H. *J. Inorg. Organomet. Polym.* **2005**, *15*, 147−156.

(14) Nijhuis, C. A.; Dolatowska, K. A.; Ravoo, B. J.; Huskens, J.; Reinhoudt, D. N. *Chem.—Eur. J.* **2007**, *13*, 69−80.

(15) Wimbush, K. S.; Reus, W. F.; van der Wiel, W. G.; Reinhoudt, D. N.; Whitesides, G. M.; Nijhuis, C. A.; Velders, A. H. *Angew. Chem., Int. Ed.* **2010**, *49*, 10176−10180.

(16) (a) Ochi, Y.; Suzuki, M.; Imaoka, T.; Murata, M.; Nishihara, H.; Einaga, Y.; Yamamoto, K. *J. Am. Chem. Soc.* **2010**, *132*, 5061−5069. (b) Cuadrado, I.; Casado, C. M.; Alonso, B.; Moran, M.; Losada, J.; Belsky, V. *J. Am. Chem. Soc.* **1997**, *119*, 7613−7614. (c) Villena, C.; Losada, J.; Garcia-Armada, P.; Casado, C. M.; Alonso, B. *Organometallics* **2012**, *31*, 3284−3291.

(17) (a) Yamamoto, T.; Morikita, T.; Maruyama, T.; Kubota, K.; Katada, M. *Macromolecules* **1997**, *30*, 5390−5396. (b) Yan, S. G.; Hupp, J. T. *J. Electroanal. Chem.* **1995**, *397*, 119−26. (c) Deraedt, C.; Rapakousiou, A.; Wang, Y.; Salmon, L.; Bousquet, M.; Astruc, D. *Angew. Chem., Int. Ed.* **2014**, *53*, 8445−8449.

(18) (a) Wang, Y.; Rapakousiou, A.; Chastanet, G.; Salmon, L.; Ruiz, J.; Astruc, D. *Organometallics* **2013**, *32*, 6136−6146. (b) Djeda, R.; Rapakousiou, A.; Liang, L.; Guidolin, N.; Ruiz, J.; Astruc, D. *Angew. Chem., Int. Ed.* **2010**, *49*, 8152−8156. (c) Astruc, D.; Liang, L.; Rapakousiou, A.; Ruiz, J. *Acc. Chem. Res.* **2012**, *45*, 630−640. (d) Poppitz, E. A.; Hildebrandt, A.; Korb, N.; Lang, H. *J. Organomet. Chem.* **2014**, *752*, 133−140. (e) Rapakousiou, A.; Djeda, R.; Grillaud, M.; Li, N.; Ruiz, J.; Astruc, D. *Organometallics* **2014**, DOI: 10.1021/om501031u.

(19) (a) Deraedt, C.; Pinaud, N.; Astruc, D. *J. Am. Chem. Soc.* **2014**, *136*, 12092−12098. (b) Deraedt, C.; Astruc, D. *Acc. Chem. Res.* **2014**, *47*, 494−503.

(20) (a) Myachina, G. F.; Konkova, T. V.; Korzhova, S. A.; Ermakova, T. G.; Pozdnyakov, A. S.; Sukhov, B. G.; Arsentev, K. Yu.; Likhoshvai, E. V.; Trofimov, B. A. *Dokl. Chem.* **2010**, *431*, 63−64. (b) Oldham, E. D.; Seelam, S.; Lema, C.; Agulera, R. J.; Fiegel, J.; Rankin, S. E.; Knutson, B. L.; Lehmler, H. *Carbohydr. Res.* **2013**, *379*, 68−77. (c) Dallmann, A.; El-Sagheer, A. H.; Dehmel, L.; Mügge, C.; Griesinger, C.; Ernsting, N. P.; Brown, T. *Chem.—Eur. J.* **2011**, *17*, 14714−14717.

(21) Rapakousiou, A.; Deraedt, C.; Gu, H.; Salmon, L.; Belin, C.; Ruiz, J.; Astruc, D. *J. Am. Chem. Soc.* **2014**, *136*, 13995−13998.

(22) Rosenberg, N.; Neuse, E. W. *J. Organomet. Chem.* **1966**, *6*, 76−85.

(23) Doisneau, G.; Balavoine, G.; Fillebeen-Khan, T. *J. Organomet. Chem.* **1992**, *425*, 113−117.

(24) Polin, J.; Schottenberger, H. *Org. Synth.* **1996**, *73*, 262−269.

(25) Zhang, K.; Tew, G. N. *ACS Macro Lett.* **2012**, *1*, 574−579.

(26) Vougioukalakis, G. C.; Georgios, C.; Grubbs, R. H. *Chem. Rev.* **2010**, *110*, 1746−1787.

(27) Liang, L.; Rapakousiou, A.; Salmon, L.; Ruiz, J.; Astruc, D.; Dash, P.; Satapathy, R.; Hosmane, N. S. *Eur. J. Inorg. Chem.* **2011**, *20*, 3043−3049.

DOI: 10.1021/ic5028916
Inorg. Chem. 2015, 54, 2284−2299

(28) (a) Rostovtsev, V. V.; Green, L. G.; Fokin, V. V.; Sharpless, K. B. *Angew. Chem., Int. Ed.* **2002**, *41*, 2596−2599. (b) Meldal, M.; Tornoe, C. W. *Chem. Rev.* **2008**, *108*, 2952−3015.
(29) Binder, W. H.; Sachsenhofer, R. *Macromol. Rapid Commun.* **2008**, *29*, 952−981.
(30) Ornelas, C.; Ruiz, J.; Cloutet, E.; Alves, S.; Astruc, D. *Angew. Chem., Int. Ed.* **2007**, *46*, 872−877.
(31) Liang, L.; Ruiz, J.; Astruc, D. *Adv. Synth. Catal.* **2011**, *353*, 3434−3450.
(32) Zhao, P.; Grillaud, M.; Salmon, L.; Ruiz, J.; Astruc, D. *Adv. Synth. Catal.* **2012**, *354*, 1001−1011.
(33) Dong, T. Y.; Chang, S. W.; Lin, S. F.; Lin, M. C.; Wen, Y. S.; Lee, L. *Organometallics* **2006**, *25*, 2018−2024.
(34) Brigger, I.; Dubernet, C.; Couvreur, P. *Adv. Drug Delivery Rev.* **2002**, *54*, 631−651.
(35) Lohan, M.; Ecorchard, P.; Rüffer, T.; Justaud, F.; Lapinte, C.; Lang, H. *Organometallics* **2009**, *28*, 1878−1890.
(36) Powers, M. J.; Meyer, T. J. *J. Am. Chem. Soc.* **1980**, *102*, 1289−1297.
(37) Ruiz, J.; Astruc, D. *C.R. Acad. Sci. t. 1, Ser. IIc* **1998**, *32*, 21−27.
(38) (a) Sutton, J. E.; Sutton, P. M.; Taube, H. *Inorg. Chem.* **1979**, *18*, 1017−1024. (b) Barrière, F.; Geiger, W. E. *Acc. Chem. Res.* **2010**, *43*, 1030−1039.
(39) Gorman, C. B.; Smith, B. L.; Parkhurst, H.; Sierputowska-Gracz, H.; Haney, C. A. *J. Am. Chem. Soc.* **1999**, *121*, 9958−9966.
(40) Amatore, C.; Bouret, Y.; Maisonhaute, E.; Goldsmith, J. I.; Abruña, H. D. *Chem.—Eur. J.* **2001**, *7*, 2206−2226.
(41) Bard, A. J.; Faulkner, L. R. *Electrochemical Methods: Fundamentals and Applications*, 2nd ed.; Wiley: New York, 2001.
(42) Flanagan, J. B.; Margel, S.; Bard, A. *J. Am. Chem. Soc.* **1978**, *100*, 4248−4253.
(43) (a) Cheon, K. S.; Kazmaier, P. M.; Keum, S. R.; Park, K. T.; Buncel, E. *Can. J. Chem.* **2004**, *82*, 551−556. (b) Liu, D.; De Feyter, S.; Cotlet, M.; Stefan, A.; Wiesler, U. M.; Herrman, A.; Grebel-Koehler, D.; Qu, J.; Müllen, K.; De Schryver, F. C. *Macromolecules* **2003**, *16*, 5918−5928.
(44) (a) Morrison, W. H.; Krogsrud, S.; Hendrickson, D. N. *Inorg. Chem.* **1973**, *12*, 1998−2004. (b) Dong, T. Y.; Hendrickson, D. N.; Iwai, K.; Cohn, M. J.; Geib, S. J.; Rheingold, A. L.; Sano, H.; Motoyama, I.; Nakashima, S. *J. Am. Chem. Soc.* **1985**, *107*, 7996. (c) McManis, G. E.; Gochev, A.; Nielson, R. M.; Weaver, M. J. *J. Phys. Chem.* **1989**, *93*, 7733−7739. (d) Nakashima, S.; Sano, H. *Hyperfine Interact.* **1990**, *53*, 367−372. (e) Gu, H.; Rapakousiou, A.; Ruiz, J.; Astruc, D. *Organometallics* **2014**, *33*, 4323−4335.
(45) (a) Haruta, M.; Date, M. *Appl. Catal., A* **2001**, *222*, 227. (b) Cao, Y. W. C.; Jin, R.; Mirkin, C. A. *Science* **2002**, *297*, 1536−1540. (c) Daniel, M.-C.; Astruc, D. *Chem. Rev.* **2004**, *104*, 293−346. (d) Myroshnychenko, V.; Rodriguez-Fernandez, J.; Pastoriza-Santos, I.; Funston, A. M.; Novo, C.; Mulvaney, P.; Liz-Marzan, L. M.; de Abajo, F. J. G. *Chem. Soc. Rev.* **2008**, 1792−1805. (e) Y. Xiong, Xia; Lim, B.; Skrabalak, S. E. *Angew. Chem., Int. Ed.* **2009**, *48*, 60−103. (f) Lal, S.; Clare, S. E.; Halas, N. J. *Acc. Chem. Res.* **2008**, *41*, 1842−1851. (g) Corma, A.; Leyva-Perez, A.; Maria Sabater, J. *Chem. Rev.* **2011**, *111*, 1657. (h) Dimitratos, N.; Lopez- Sanchez, J. A.; Hutchings, G. J. *Chem. Sci.* **2012**, *3*, 20−44. (i) Herves, P.; Perez-Lorenzo, M.; Liz-Marzan, L. M.; Dzubiella, J.; Lu, Y.; Ballauff, M. *Chem. Soc. Rev.* **2012**, *41*, 5577−5587. (j) Buck, M. R.; Schaak, R. E. *Angew. Chem., Int. Ed.* **2013**, *52*, 6154−6178. (k) Li, N.; Zhao, P.; Astruc, D. *Angew. Chem., Int. Ed.* **2014**, *52*, 1756−1789. (l) Wang, H.; Song, X.; Liu, C.; He, J.; Chong, W. H.; Chen, H. *ACS Nano* **2014**, *8*, 8063−8073.
(46) (a) Wang, X. S.; Wang, H.; Coombs, N.; Winnik, M. A.; Manners, I. *J. Am. Chem. Soc.* **2005**, *127*, 8924−8925. (b) Wang, H.; Wang, X.; Winnik, M. A.; Manners, I. *J. Am. Chem. Soc.* **2008**, *130*, 12921−12930.
(47) (a) Huo, J.; Wang, L.; Yu, H.; Deng, L.; Ding, J.; Tan, Q.; Liu, Q.; Xiao, A.; Ren, G. *J. Phys. Chem. B* **2008**, *112*, 11490−11497. (b) Takahashi, S.; Anzai, J. I. *Materials* **2013**, *6*, 5742−5762. (c) Abruña, H. D. In *Electroresponsive Molecular and Polymeric Systems*: Skotheim, T. A., Ed.; Dekker: New York, 1988; Vol. *1*, p 97. (d) Murray, R. W. In *Molecular Design of Electrode Surfaces*; Murray, R. W., Ed.; Techniques of Chemistry XXII; Wiley: New York, 1992; p 1.
(48) (a) Peerce, P. J.; Bard, A. J. *J. Electroanal. Chem.* **1980**, *114*, 89−111. (b) Lenhard, J. R.; Murray, R. W. *J. Am. Chem. Soc.* **1978**, *100*, 7870−7875. (c) Brown, A. P.; Anson, F. C. *Anal. Chem.* **1977**, *49*, 1589−1595. (d) Laviron, E. *J. Electroanal. Chem.* **1981**, *122*, 37−44.

DOI: 10.1021/ic5028916
Inorg. Chem. 2015, 54, 2284−2299